

**DESIGN AND DEVELOPMENT OF WEB-BASED 3D POINT CLOUD
SCANNER SYSTEM FOR FLOUR STORAGE BIN VOLUMETRIC
MEASUREMENT**

A THESIS

Presented to the Faculty of
Department of Computer Applications
College of Computer Studies
Mindanao State University – Iligan Institute of Technology

In Partial Fulfillment
of the Requirements for the Degree
MASTER OF SCIENCE IN COMPUTER APPLICATIONS

JAAFAR J. OMAR

May 2024



Mindanao State University
ILIGAN INSTITUTE OF TECHNOLOGY
Iligan City, 9200 Philippines

SCHOOL OF GRADUATE STUDIES

CERTIFICATE OF PANEL APPROVAL

The masteral thesis attached hereto, entitled "**DESIGN AND DEVELOPMENT OF WEB-BASED 3D POINT CLOUD SCANNER SYSTEM FOR FLOUR STORAGE BIN VOLUMETRIC MEASUREMENT**", was prepared and submitted by **JAAFAR J. OMAR**, in partial fulfillment for the degree of **MASTER OF SCIENCE IN COMPUTER APPLICATIONS**, is hereby recommended for approval.

LEAH A. ALINDAYO, D.Eng.

Member

MARIA FE BAHINTING, MIT

Member

Date

Date

CARL JOHN O. SALAAN, PhD

Adviser

EARL RYAN M. ALELUYA, MSc

Co-Adviser

Date

Date

This thesis is approved in partial fulfillment of the requirements for the degree of **MASTER OF SCIENCE IN COMPUTER APPLICATIONS**.

ERIK LOUWE R. SALA, MSIT

Graduate Coordinator

RABBY Q. LAVILLES, DIT

College Dean

Date

Date

ABSTRACT

Adequate monitoring of flour storage bins in the food manufacturing industry is crucial to prevent profit loss from underproduction and overstocking. Underproduction can lead to stockouts and profit loss, while overstocking increases the risk of spoilage and contamination by flour beetles. Infestation in products and raw materials can cost manufacturers up to 3.60% of the total Cost of Quality. Additionally, manual volume measurement is labor-intensive and error-prone, highlighting the need for efficient monitoring.

This study presents the design and development of volumetric measurement using Web-based 3D Point Cloud Scanner System attached at the top of storage bin to scan and automatically measure the empty space and product volume inside of a storage. The successful integration and actual testing of the system highlighted the effectiveness and efficacy in a real-world setting. The inclusion of the web application provided functionalities such as remote scanning and volume monitoring to address the manual and laborious measurement method.

Keywords—automation, web application, ROS, point cloud scanner, volume measurement

*This work is lovingly dedicated to
God Almighty (Allah)*

©

To My loving Family and Friends

ACKNOWLEDGEMENT

My heartfelt thanks go to the following individuals for their invaluable contributions to the completion of this study and to my roller coaster master's journey:

First and foremost, to my adviser and co-adviser, Prof. Carl John O. Salaan and Prof. Earl Ryan M. Aleluya, for their unwavering support, direction, motivation, and guidance throughout this research journey. I also extend my gratitude to my panels, Prof. Alindayo and Prof. Bahinting, for their invaluable inputs and suggestions, which helped me refine my research significantly.

I am deeply thankful to my classmates, Nouran Usman, Melody Mae Maluya, Jamaica Mae Pepito, Collien Princess Pepito, Ryan Himongala, and Rochelle Madulara, for their support, laughter, memorable travels, and cherished memories. A special thanks to the Control and Robotics Laboratory family: ma'am Jam, sir Imman, kuya Joey, ma'am Pao, and sir Steve, for their assistance and contributions.

I am also grateful to my Dormitory family, too many to mention individually, for our bonding, support, and the countless memories we shared.

I extend my sincere thanks to the Department of Science and Technology - Engineering Research and Development for Technology for their financial support, with a special mention to Ma'am Doruthee for processing

our allowances and addressing other financial and scholar concerns.

Most importantly, I owe a profound debt of gratitude to my ina (mother) and ama (father), Maryam Omar and Usman Omar Jr., for their unconditional love, understanding, care, moral support, and prayers.

Above all, I thank Allah the Mighty and the Majestic for His guidance and for bestowing upon me the knowledge, wisdom, patience, and strength required to complete this work.

Jaafar J. Omar

TABLE OF CONTENTS

TITLE PAGE	i
APPROVAL SHEET	ii
ABSTRACT	iii
DEDICATION	iv
ACKNOWLEDGEMENT	v
TABLE OF CONTENTS	vii
LIST OF FIGURES	xiii
LIST OF TABLES	xvi
I Introduction	1
1.1 Background of the Study	1
1.2 Statement of the Problem	3
1.3 Objectives of the Study	4
1.4 Originality of the Study	5
1.5 Scope and Limitations	5
1.6 Significance of the Study	6
1.7 Conceptual Framework	6
1.8 Theoretical Framework	8
1.8.1 Calculating Storage Materials Volume using Depth Mea-	
surement	8

1.8.2	3D Polar Coordinate to Cartesian Coordinate	9
1.8.3	Point Cloud Data	10
1.8.4	Computational Geometry using Convex Hull	10
1.8.5	ROS Nodes, Topics, and Subscribe-Publish Relationship	12
1.9	Definition of Terms	13
II	Review of Related Literature	15
2.1	Overview of Existing Methods, Techniques and Technologies Used for Volume Measurement	15
2.2	Point Cloud Acquisition Devices	17
2.2.1	Light Detection and Ranging (LiDAR)	18
2.2.2	Rotating 2D LiDAR Scanner into a 3D Point Cloud Scanner: Mechanisms and Techniques	20
2.3	Volume Measurement Using 3D Point Cloud Data	23
2.3.1	Frameworks for Point Cloud Processing, Visualization, and Mapping	23
2.3.2	Techniques and Methods for Volume Estimation Us- ing Computational Geometry	24
2.4	Robot Web Tools Application for ROS Remote Monitoring . .	27
2.5	Synthesis of the Study	28
III	Methodology	34
3.1	3D Point Cloud Scanner System Development	35

3.1.1	Hardware Development	36
3.1.1.1	2D LiDAR Scanner	36
3.1.1.2	Rotating Mechanism	37
3.1.2	Software Development	39
3.1.2.1	Operating System and Frameworks	41
3.1.2.2	Startup Initialization Process	42
3.1.2.3	System Scanning Process	43
3.1.2.4	Volume Measurement Process	45
3.2	Web Application Development	48
3.2.1	Different Tools and Framework	48
3.2.2	Dashboard Development	50
3.2.3	Overall System Integration	50
3.3	System Testing and Evaluation	52
3.3.1	LiDAR and Servo Calibration Test	52
3.3.2	System Volume Measurement Calibration Test	53
3.3.2.1	Testing Setup	53
3.3.2.2	Empty Storage Volume Measurement Calibration	55
3.3.2.3	Different Volume Quantity Measurement Calibration	55
3.3.2.4	Volume Measurement Using the System and Sounding Method Test	56

3.3.3	System Evaluation	57
3.3.3.1	LiDAR Range Evaluation	57
3.3.3.2	Servo Angle Evaluation	57
3.3.3.3	Empty Storage Bin Volume Measurement Evaluation	58
3.3.3.4	Different Volume Quatity Measurement Evaluation	58
3.3.3.5	Comparison Evaluation of the System and Sounding Method	59
IV Result and Discussion		60
4.1	3D Point Cloud Scanner System	60
4.1.1	Actual Prototype of the 3D Point Cloud Scanner System	62
4.1.2	Software Development Result	63
4.2	Web Application Implementation	68
4.2.1	Overall System Integration	71
4.3	System Testing and Evaluation Result	71
4.3.1	LiDAR and Servo Calibration Test Result	71
4.3.1.1	LiDAR Range Calibration	72
4.3.1.2	Servo Angle Calibration	72
4.3.2	System Volume Measurement Calibration Result	73
4.3.2.1	Testing Setup Result	73

4.3.2.2	Empty Storage Volume Measurement Calibration Test Result	76
4.3.2.3	Different Volume Quantity Measurement Calibration Test Result	79
4.3.2.4	Volume Measurement Using the System and Sounding Method Result	85
4.3.3	System Evaluation	88
4.3.3.1	LiDAR Calibration Evaluation	88
4.3.3.2	Servo Calibration Evaluation	88
4.3.3.3	Empty Storage Volume Measurement	89
4.3.3.4	Different Volume Quantity Measurement	89
4.3.3.5	Comparison Evaluation of the System and Sounding Method	90
V	Conclusion and Recommendation	91
5.1	Conclusion	91
5.2	Recommendations	92
REFERENCES		92
APPENDICES		99
A	Components Specification	100
B	Testing Documentation	105

C STATISTICAL DATA	117
---------------------------	------------

CERTIFICATE OF AUTHENTIC AUTHORSHIP	119
--	------------

LIST OF FIGURES

1.1	General Conceptual Flow	7
1.2	LiDAR Scan Range Conversion from Polar Coordinates (ρ, θ, ϕ), to Cartesian Coordinate (x, y, z)	10
1.3	Convex Hull of Set of Points	12
2.1	Typical LiDAR System	19
2.2	360-degree scan of 2D LiDAR	20
2.3	Four different configurations for rotating: (a) pitching scan, (b) rolling scan, (c) yawing scan, (d) top yawing scan	21
2.4	Convex Hull	26
3.1	System Architecture Block Diagram: (A) 3D Point Cloud Scanner System, (B) Web Application	34
3.2	System Development Process	35
3.3	3D Point Cloud Scanner Development Flow Chart	36
3.4	Scan Direction of LiDAR and Movement Direction of the Servo	38
3.5	Synchronization Process of LiDAR and Servo	39
3.6	Nodes, Topics and their Relationships	40
3.7	Flow Chart of the Different Software Processes	41
3.8	System Idle Mode Process Flow Chart	43

3.9	From Scanning to Mapped Point Cloud Data Flow Chart	45
3.10	Flow Chart of the System's Volume Measurement Process	47
3.11	Process Flow Chart of Scanner System and Web App	50
3.12	Communication Protocol of the Web Interface and the System	52
3.13	CAD Model Design of the Storage Bin	54
4.1	Different View of the CAD Model Design of 3D Point Cloud Scanner System	61
4.2	Specific Components of the System	61
4.3	Actual 3D Point Cloud Scanner System Developed	62
4.4	Actual Circuit Components of the System	63
4.5	Example of the Volume Estimation Process of the System	67
4.6	Main Dashboard	69
4.7	Data Section	70
4.8	Single Database Schema of the Web Application	71
4.9	Actual Flour Storage Bin Created	75
4.10	Testing Field and The Actual System Setup	76
4.11	Actual Empty Bin and Scanned Point Cloud Data	77
4.12	Actual Web Visualization of Point Cloud and Volume	77
4.13	Container with a Known Volume Used for Testing	80
4.14	Actual and Point Cloud Surface Contour of Test 1	80
4.15	Actual and Point Cloud Surface Contours of Test 2	82

4.16 Actual and Point Cloud Surface Contour of Test 3	84
4.17 Distribution of volume measurements obtained from the sys- tem and sounding	86

LIST OF TABLES

2.1 Point Cloud Volume of Different Model	27
2.2 Research Synthesis Matrix	31
3.1 Tools and Frameworks Used in the Web Application	49
4.1 LiDAR Range Calibration Results	72
4.2 Sevo Angle Calibration Results	73
4.3 Individual and Total Volume of the Storage Bin	74
4.4 Actual and Measured Volume of Empty Storage Bin Volume Measurement Result	78
4.5 Volume Measurements Calibration Result of the System Across Two Contours with A Known Volume of $0.0594\ m^3$	81
4.6 Volume Measurements Calibration Result of the System Across Two Contours with A Known Volume of $0.4752\ m^3$	83
4.7 Volume Measurements Calibration Result of the System Across Two Contours with A Known Volume of $0.7128\ m^3$	85
4.8 Comparison of Volume Measurement Using the 3D Point Cloud Scanner System and Traditional Sounding Method for Differ- ent Surface Contours	87

C.1 One Sample-test for Actual and Measured Volume of Empty Storage Bin Volume Measurement Result	117
C.2 ANOVA Results of Volume Measurements Calibration Result of the System Across Two Contours with A Known Volume of $0.0594\ m^3$	117
C.3 ANOVA Results of Volume Measurements Calibration Result of the System Across Two Contours with A Known Volume of $0.4752\ m^3$	117
C.4 ANOVA Results of Volume Measurements Calibration Result of the System Across Two Contours with A Known Volume of $0.7128\ m^3$	117
C.5 One Sample-test for Comparison of Volume Measurement of the System VS. Sounding Method	118

CHAPTER I

INTRODUCTION

1.1 Background of the Study

Agricultural raw materials, such as rice, wheat, and corn, which mostly include solid, liquid or powdered, provide significant amounts of carbohydrates for use in industry and human nutrition . Certain grains require little processing and can be eaten right away after harvest, while others must be prepared through a number of primary and secondary milling steps. As farmers learned to produced more resulting of various agricultural innovation, this raw materials must preserve the quality for future consumption (Bucklin et al., 2019). It is expected an increase in raw materials annually does necessitate an efficient post-harvest processes such as raw product storing method incorporating modern technologies (Kumar and Kalita, 2017; Yegorova et al., 2021; Munarso et al., 2022).

Various tools and methods have been developed to measure stored raw materials volume inside an industrial storage silos or bins, employing sensors like contact level indicators (e.g., tilt switches, pressure diaphragms, rotary paddles) and non-contact indicators (e.g., stereovision, radar, ultrasound, lasers). Contact sensors offer cost-effective, dust-resistant point mea-

surements but lack surface detail. Non-contact sensors can map grain surfaces accurately but require permanent mounting, are relatively expensive, and are susceptible to dust interference. However, conventional volumetric measurement method using weighted fiberglass tape is still being used providing only a single data point which leads to inaccuracy and error-prone volume measurement (Turner et al., 2016, 2017).

Point cloud data consists of a set of points representing an object in either a two or three-dimensional structure. This data typically comprises X, Y, and Z coordinates, but modern point clouds may also include additional information such as intensity, RGB values, and more (Wang and Kim, 2019; Stojanovic, 2023).

Light Detection and Ranging (LiDAR) is one of the many devices that can gather 3D points that often refer as point clouds. Unfortunately, commercial 3D LiDAR systems tend to be expensive in comparison to their 2D-based LiDAR. This cost disparity can lead to limitations in accessibility for certain applications or industries, hindering widespread adoption and innovation in fields where 3D spatial data is crucial. Low-cost two axes-based LiDAR can mimic the collection of 3D point cloud by adding an additional axes using tilting device (Clar and Salaan, 2022). However, it comes with a notable drawback: it lacks several capabilities present in high-end 3D LiDAR systems, including multi-echo functionality, long-range detection, high angular resolution, among others.

Recent innovations in various industries have made the production less manual but producing more by using automation and wireless technologies that helped to produce better and accurate measurement compared to traditional methods. These approaches include various sensing technologies, automated measurements, machine to machine (M2M) communications, and monitoring systems. The interconnected sensors and actuators allow to remotely collect data, store, and process the data to provide better insight in the industry and also for the economic growth, specify the characteristics of a paperless factory, it is a development of a smart factory in which all data that is turned into information is stored, transferred, and displayed entirely remotely and digitally. As the level of digitization of a smart factory, it is not a revolution but rather an evolution (Bulut et al., 2020).

1.2 Statement of the Problem

While some food manufacturing industries still rely on manual and labor-intensive storage measurement procedures, there is a growing need to adopt advanced technologies with remote capabilities. This shift aims to eliminate the need for frequent physical processes that may endanger employees. Additionally, monitoring the volume of raw product storage, particularly in industries dealing with essential commodities like flour, holds paramount importance for various reasons. Ensuring accurate and timely monitoring of storage bins prevents detrimental scenarios such as under-

production or overstocking. In the case of underproduction, inadequate monitoring leading to stockouts can disrupt the production process, resulting in delayed deliveries and potential loss of sales. Conversely, overstocking can lead to unnecessary inventory costs, space constraints, and increased risk of product spoilage or infestation. Specifically, in the context of flour storage, overstocking can attract flour beetles, leading to infestation and contamination of the stored flour when left unsold. Thus, precise volume monitoring is crucial to maintaining optimal inventory levels, facilitating efficient production planning, and mitigating the risk of financial losses and product quality issues for food manufacturing industries. One challenging factor in developing technology in this area is ensuring the system's accuracy while maintaining a compact and portable design for easy integration and installation.

This study presents the development of a volumetric measurement system for flour storage bin. The system is designed to be controlled and scanned remotely using a web-based interface.

1.3 Objectives of the Study

The general objective of this study was to develop a system that can measure the volume of the product inside of a flour storage bin. The following specific goals were completed:

1. Developed a 3D point cloud scanner system.
2. Developed a web-based application that can send a command to the system and visualization for point cloud and volume measurement;
3. Tested and evaluated the performance of the system.

1.4 Originality of the Study

The originality of this study lies from addressing existing gaps in volume estimation and monitoring systems for flour storage bins, in the development of a system capable of estimating and monitoring the volume and capacity of flour storage bin. The contribution of this study to the scientific community are the following:

- Development of 3D Point Cloud Scanner System specifically for measuring the volume of flour materials within storage bins.
- Development of web-based application integrated to the system for point cloud and volume visualization.

1.5 Scope and Limitations

The scope and limitations of this study are the following:

- The aim of the study is to develop a volume measurement intended for flour storage bin.

- The conducted testing of the system was not done to any commercial manufacturing industry.
- The study focuses on utilizing flour as the primary raw material for testing purposes.

1.6 Significance of the Study

Accurate and efficient post-harvest processes are vital in the food industry to ensure effective inventory management and maintain an adequate supply of materials. Volume measurement automation can be integrated into a variety of industries, eliminating labor-intensive tasks that may expose employees to dangerous scenarios. The development of the 3D point cloud scanner system (3D-PCSS) addresses the need for precise volume measurement of stored flour within flour storage bin. Furthermore, the testing and evaluation of the system provide valuable insights into its performance and potential for further development.

1.7 Conceptual Framework

Figure 1.7 outlines the conceptual framework of the study. As illustrated in the figure, the study's general concept involves placing the system at the top of the flour bin and controlling it through the web application. The volume of the flour materials is determined by scanning the empty space

within the flour bin and generating 3D point cloud data of the empty space. Finally, the point cloud data and measured volume are displayed in the web application.

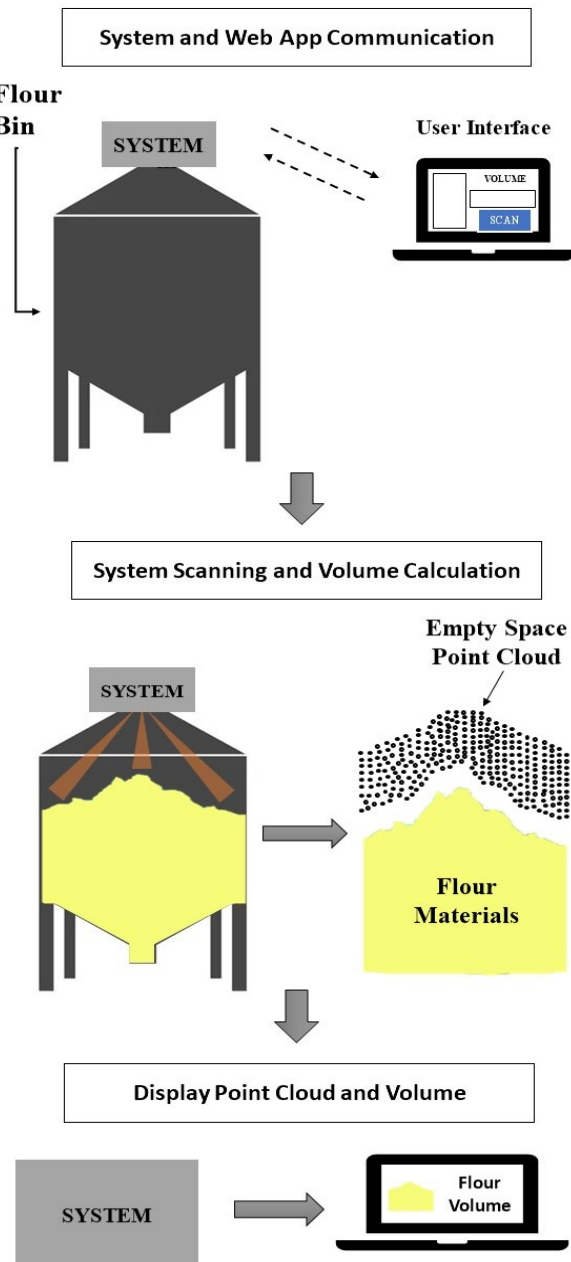


Figure 1.1. General Conceptual Flow

1.8 Theoretical Framework

This section introduces the fundamental theories that guides the underlying principles, methodologies and technologies involved in the study.

1.8.1 Calculating Storage Materials Volume using Depth Measurement

The volume of stored grain is typically calculated using the depth measurement. Once the equivalent level height of the grain is determined based on the depth measurement and surface profile assessment, this height is multiplied by the conversion factor to obtain the volume of the stored grain. This calculation accounts for the headspace between the eave and the grain surface. The underlying calculation with a single and non complex geometric shape can be presented as follows:

$$V = A \cdot h \quad (1.1)$$

Where:

V : Volume of the storage container

A : Area of the base of the container

h : Height or depth of the container

1.8.2 3D Polar Coordinate to Cartesian Coordinate

Converting polar coordinates to cartesian coordinates in three dimensions involves considering the radial distance (ρ), the polar angle (θ), and the azimuthal angle (ϕ). Given a point in spherical coordinates (ρ, θ, ϕ) , the corresponding Cartesian coordinates (x, y, z) can be calculated as follows:

$$x = \rho \cdot \sin(\theta) \cdot \cos(\phi) \quad (1.2)$$

$$y = \rho \cdot \sin(\theta) \cdot \sin(\phi) \quad (1.3)$$

$$z = \rho \cdot \cos(\theta) \quad (1.4)$$

Where: x , y , and z represent the Cartesian coordinates of the point. ρ is the radial distance from the origin to the point. θ is the polar angle measured from the positive z -axis to the point. ϕ is the azimuthal angle measured from the positive x -axis to the projection of the point onto the xy -plane.

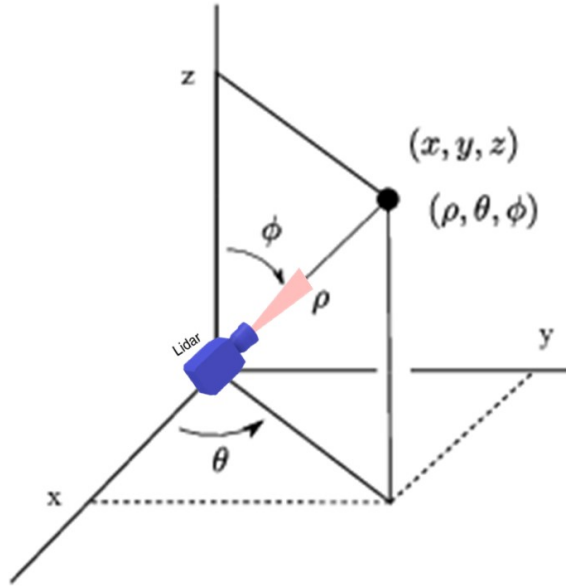


Figure 1.2. LiDAR Scan Range Conversion from Polar Coordinates (ρ, θ, ϕ) , to Cartesian Coordinate (x, y, z)

1.8.3 Point Cloud Data

A set of points in three dimensions that represent an object's or scene's surface is called a point cloud. Point clouds can be generated through a variety of methods, including photogrammetry, LiDAR, and 3D scanning. Processing and evaluation of these point clouds for a variety of applications is an increasing area of point cloud processing.

1.8.4 Computational Geometry using Convex Hull

The study of the development and evaluation of algorithms for geometric problems in low dimensions—usually two or three—is known as computational geometry. As the smallest convex polygon containing a given

set of points, the Convex Hull is a fundamental concept in computational geometry. The convex hull represents the smallest convex set enclosing a given set of points in a Euclidean space as figure 1.3 illustrated. It adheres to principles of convexity, ensuring that the shape remains convex, and minimality, guaranteeing it encompasses the points with minimal expansion.

The Gift Wrapping algorithm, which has a time complexity of $O(nh)$, where n is the number of points and h is the number of points on the hull, is one straightforward method for calculating the Convex Hull.

The equation 1.5 defines the convex hull of a set of points P_j in N -dimensional space. The variable C represents a point in the convex hull, λ_j are non-negative weights, and A_j are some constraints. The summation iterates over all points from $j = 1$ to N .

$$C = \left\{ \sum_{j=1}^N \lambda_j P_j : \lambda_j \geq 0 \text{ for all } j \text{ and } \sum_{j=1}^N \lambda_j = 1 \right\} \quad (1.5)$$

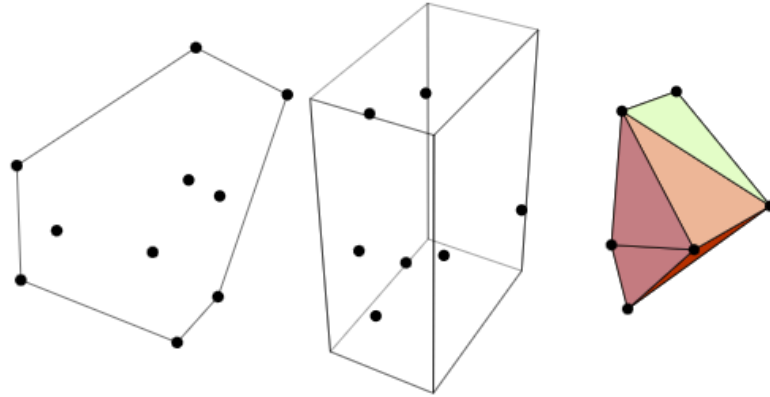


Figure 1.3. Convex Hull of Set of Points

1.8.5 ROS Nodes, Topics, and Subscribe-Publish Relationship

A framework for building complicated robotic systems that is adaptable is called Robot Operating System (ROS). It makes it possible for nodes, software components that carry out particular functions, to communicate with one another. Topics, also referred to as buses, are the methods by which nodes exchange messages with one another. A key component of ROS is the publish-subscribe connection, in which nodes can publish or subscribe to topics.

Nodes in ROS have the ability to simultaneously subscribe to an indefinite number of topics and share data to an indefinite number of topics. One of the main methods of data communication between nodes, and consequently between other components of the system, is through topics (St-Onge and Herath, 2022). A node must first advertise a topic before pub-

lishing content, or messages, into it in order to exchange information. The first part is completed in the node's initialization code, and the second is completed each time new data has to be shared, usually at a predetermined frequency inside the main loop of the code. Conversely, the node or nodes that need the content of a topic will subscribe to it. The subscriber will associate a callback function triggered for each new incoming message (St-Onge and Herath, 2022).

1.9 Definition of Terms

1. **LiDAR**—stands for Light Detection and Ranging, can also be described as Light Imaging, Detection, and Ranging. It is a method for determining ranges by targeting an object or a surface with a laser and measuring the time-of-flight to determine the distance.
2. **Bin** —is a large container used to store materials, such as grain, coal, sand, or other bulk goods. They are typically made of metal, plastic, or wood and come in various sizes, shapes, and designs.
3. **ROS** —Robot Operating System is a set of open-source libraries and tools designed to help developers build robot applications. It provides a common framework for creating, managing and sharing code, data, and other resources related to robotic systems.
4. **Point Cloud** —is a set of data points in a three-dimensional space,

typically representing the surface of an object. Each point in the cloud is defined by its three-dimensional coordinates (x, y, and z) and may also include additional information such as color, intensity, or normal vector.

5. **Convex Hull** —is the minimum convex polygon from the set of points that encompasses all of the points in the set.

CHAPTER II

REVIEW OF RELATED LITERATURE

Enhancing post-harvest processing and storage technology is essential meeting increasing global demand and minimizing waste. Improved technology ensures efficient supply chains and reduces losses due to spoilage, damage, or inefficient methods. Moreover, advanced monitoring and management techniques not only enhance production but also contribute to safety standards (Kumar and Kalita, 2017; Munarso et al., 2022).

In this chapter, various relate topic were reviewed and discussed. Different methods, technologies and implementation were also introduced and examined.

2.1 Overview of Existing Methods, Techniques and Technologies Used for Volume Measurement

According to Turner et al. (2016), the determination of grain volume in a bin depends on variables like bin diameter and corresponding level height of grain. Different surface condition assessment, however, is subjective and subject to a number of variables, such as operator experience, visibility, lighting, and ambient circumstances. Various strategies can be used to improve volume estimate; standard angles of repose for various grain types

are provided in the literature.

Traditional level measurements are already used and studied in different industries such as weight and cable methods, ultrasonic, Guided Ware Radar (GWR), and Thru-air Radar (TAR) which has their own advantage and disadvantages. Ultrasonic and laser technologies are excellent in providing accurate and detailed measurement of level. However, these technologies are problematic when in terms of dusty environment (Duysak and Yigit, 2020). Additionally, Various tools and methods have been developed to measure stored raw materials volume inside an industrial storage silos or bins, employing sensors like contact level indicators (e.g., tilt switches, pressure diaphragms, rotary paddles) and non-contact indicators (e.g., stereovision, radar, ultrasound, lasers). Contact sensors offer cost-effective, dust-resistant point measurements but lack surface detail. Non-contact sensors can map grain surfaces accurately but require permanent mounting, are relatively expensive, and are susceptible to dust interference. However, conventional volumetric measurement method using weighted fiberglass tape is still being used providing only a single data point which leads to inaccuracy and error-prone volume measurement due to uneven materials surface topology (Turner et al., 2016, 2017).

New methods and technologies have been trying to incorporate in industrial settings to enhance the measurement methods such as using Microwaves Radar (Vogt and Gerdin, 2017), Horn Antennas-based (Duysak

and Yigit, 2020; Yigit et al., 2015), Load Cell, Ultrasonic, Laser-based (Guevara et al., 2020), and Temperature-based sensor (Rhee et al., 2021).

2.2 Point Cloud Acquisition Devices

The recent advancements in spatial acquisition technologies such as 3D laser scanning, photogrammetry, videogrammetry, RGB-D camera, and stereo camera have resulted in the formation of point clouds that may contain millions, billions, or trillions of points (Jaboyedoff et al., 2012). Various 3-dimensional scanning technology produces data that are formatted as point cloud, typically these point cloud data acquired using laser or image scanner. These gathered data can be managed to ease the measurement and visualization of an object or environment (Chua et al., 2017). Point cloud data are processed to generate desired output on the specific application. Over the past 20 years, the advent of high-quality 3D point cloud acquisition changes the perspective of robotics. Moreover, 3D scanning through various technologies enable the possibility of less contact for physical measurement that eliminate the traditional approach that involves time and effort. These technologies vary in size, functionality, and cost, ranging from affordable options to more complex and expensive ones (Rusu and Cousins, 2011).

2.2.1 Light Detection and Ranging (LiDAR)

LiDAR, a remote sensing technology, employs laser light to create precise 2D or 3D models of objects or environments. Apart from Time-of-Flight (ToF) and triangulation, which measures distances based on the angle and timing of laser pulses, LiDAR systems utilize other techniques such as amplitude modulation and frequency modulation. These techniques vary in how they measure distances and capture data. By integrating data from multiple laser pulses, LiDAR generates a comprehensive point cloud that accurately represents the shape and structure of the objects within the environment, Figure 2.1 shows the block diagram of a typical LiDAR system. LiDAR technology have been used in industrial settings. In the context of LiDAR scanning, individual point cloud scans are acquired and processed for a specific area. These point clouds are then merged and blended together to generate a complete point cloud of the desired area, which can be utilized for distance and measurement calculations (Jaboyedoff et al., 2012; Raj et al., 2020).

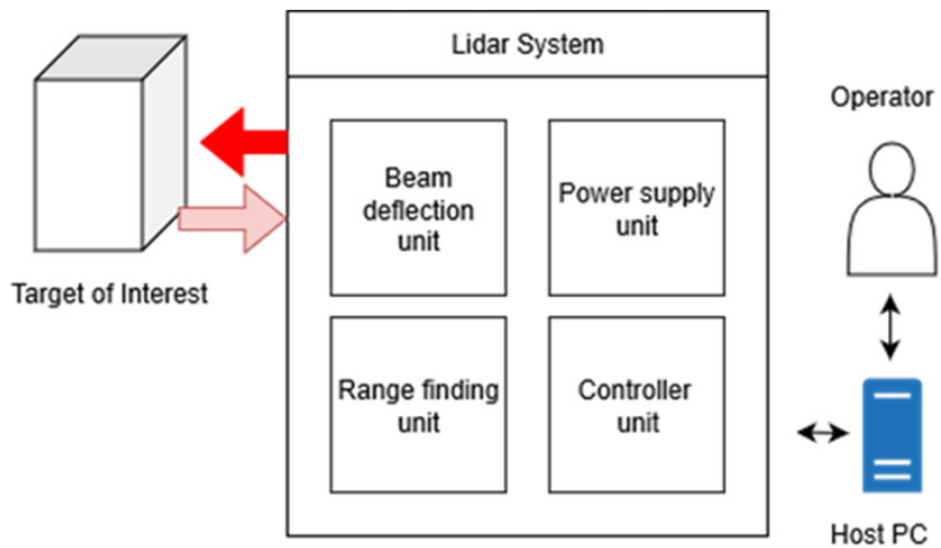


Figure 2.1. Typical LiDAR System

A 360-degree scan of a LiDAR is generally obtained as shown in figure 2.2 to produce a 2D map, a typical scan using the robot's top-mounted 2D LIDAR. The axis of the rotating LIDAR sensor is shown as a red line. The border of the surrounding obstacles is indicated in blue (Sarker et al., 2020).

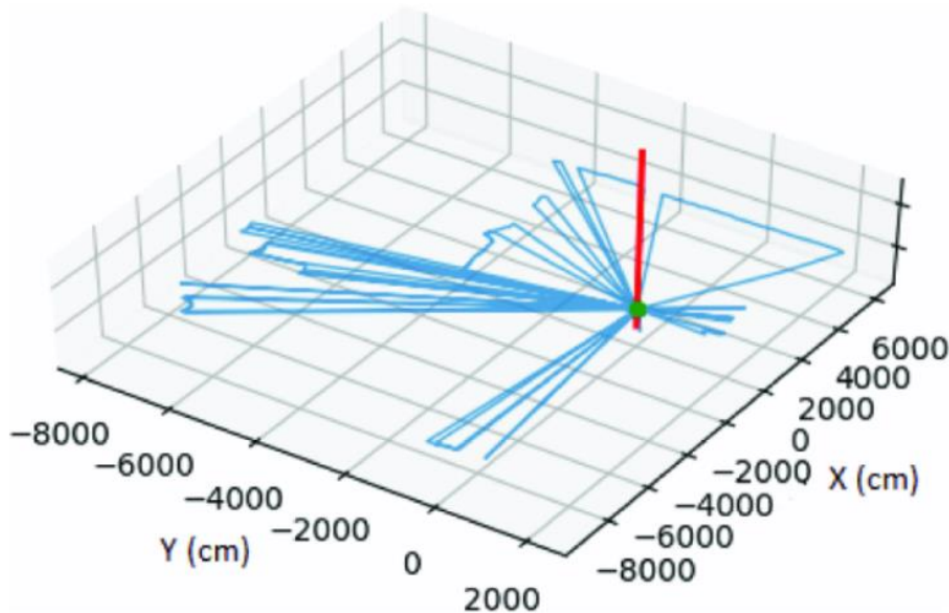


Figure 2.2. 360-degree scan of 2D LiDAR

2.2.2 Rotating 2D LiDAR Scanner into a 3D Point Cloud Scanner: Mechanisms and Techniques

A 2D LiDAR scanner, typically used for horizontal plane scanning, can be transformed into a 3D point cloud scanner with the addition of extra components and processing techniques. One common method involves incorporating a rotating mechanism, such as a pan-tilt unit (PTU), to the 2D LiDAR. As the LiDAR rotates, it collects data points at various angles, generating a series of 2D scans. These scans are then combined and processed using algorithms to reconstruct a 3D representation of the surroundings. Integrating the 2D LiDAR device with electric motors into various configurations enables the acquisition of 3D scans. Figure 2.3 illustrates four such

configurations: pitching, rolling, yawing, and top yawing scans (Raj et al., 2020).

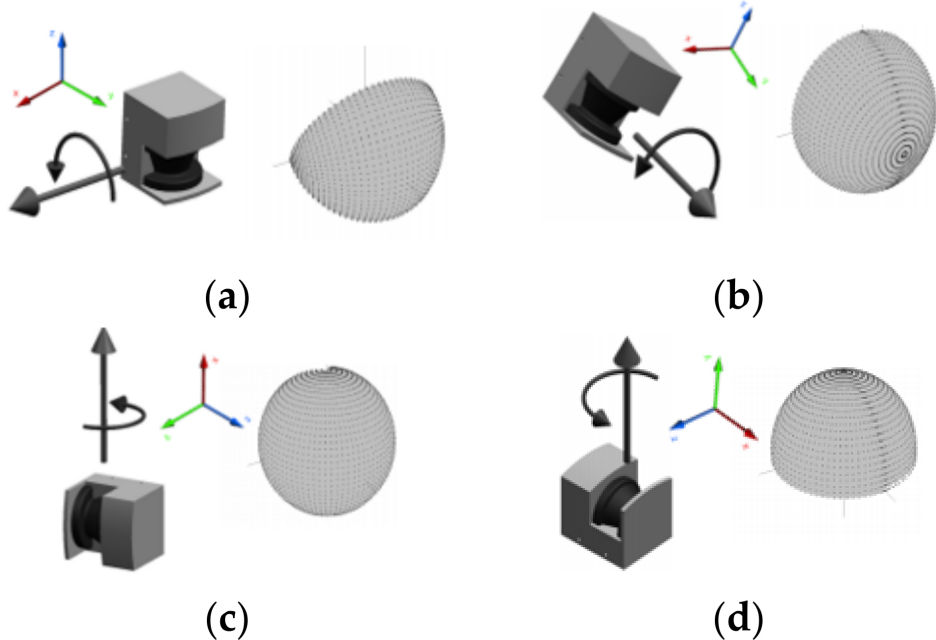


Figure 2.3. Four different configurations for rotating: (a) pitching scan, (b) rolling scan, (c) yawing scan, (d) top yawing scan

Source: (Raj et al., 2020)

Kang et al. (2018) utilized a 2D low-cost off-the-shelf LiDAR to reconstruct complex 3D model by integrating an external rotary for additional dimension. The experimental test achieved to evaluate 3D reconstruction by concluding that using a low-cost 2D LiDAR sensors can perform 3D point cloud acquisition but increase either the complexity of its hardware or software.

A stepper motor was used in the study conducted by Yuan et al. (2021) and Kang et al. (2018) to rotate a 2D LiDAR. However, in the study con-

ducted by Yuan et al. (2021), the rotating 2D LiDAR with initial motor shaft position defined using a combination of photoelectric switches and shading sheets, to create a 3D point cloud representation of the environment. The main objective of the study was to minimize the cost by utilizing stepper motor. Intensive calibration was conducted to correct the error of the system due to lack of the absolute angle position of the motor, thus, the study focus on calibrating the system by synchronizing the 2D LiDAR with the stepper motor.

In a previous study by Clar and Salaan (2022), a servo motor was employed to rotate a 2D LiDAR, with calibration performed to synchronize the LiDAR's movement. However, the system in that study relied on a laptop and microcontroller for operation. While adequate for small-scale and laboratory experimental testing, this setup posed challenges for larger-scale deployment due to its size, weight, and power demands. Consequently, there arose a need for a more compact and portable solution to address these limitations.

The primary problem with calibration and synchronization between a 2D lidar and a servo arises from the lack of an absolute angle reference for the servo. Unlike encoders or sensors that provide precise angular measurements, servos typically lack absolute positioning capabilities. Although rotating 2D LiDAR can never replace commercial 3D LiDAR with several reasons, however, rotating 2D LiDAR can be partially used and installed

with in terms of static and nonmoving environment (Bi et al., 2021).

2.3 Volume Measurement Using 3D Point Cloud Data

Utilizing the latest advances in volume measurement with 3D point cloud data is an innovative method that precisely determines the volume of spaces or objects in a three-dimensional environment. This technique makes precise and thorough volumetric analysis possible by using point cloud data, which frequently consists of millions of points in 3D space. The concepts, procedures, and uses of volume measurement with 3D point cloud data will be covered in explain in this section, along with examples of its relevance in various domains (Zhi et al., 2016; Meng et al., 2023).

2.3.1 Frameworks for Point Cloud Processing, Visualization, and Mapping

Various point cloud processing and mapping frameworks are widely available to lessen the complexity of handling raw point cloud data, such as, Robotic Operating System (ROS), Point Cloud Library (PCL), Open3D, MeshLab, etc. Most of this framework can be used in many different fields such as virtual reality, construction, industry, and surveying.

The PCL has a built-in visualization library that uses Visualization ToolKit (VTK) as its foundation. VTK is a versatile platform that can render 3D point clouds and surfaces, and supports visualizing tensors, textures,

and volumetric methods. The PCL Visualization library aims to merge PCL with VTK by providing a complete visualization layer for n-D point cloud structures. Its main goal is to allow for rapid prototyping and visualization of algorithm results on high-dimensional data (Rusu and Cousins, 2011).

Ocando et al. (2017) take advantage of using ROS framework to map the 3D point cloud data, as the framework allows to interlink programs that is written in different languages. The study successfully addressed the problematic tasks of Simultaneous Localization and Mapping (SLAM) and 3D Octomapping via single sensor. Clar and Salaan (2022) also utilizes ROS framework and PCL to filter, convert and measure the volume of the gathered point cloud data.

2.3.2 Techniques and Methods for Volume Estimation Using Computational Geometry

Point clouds in 3D are highly valuable as they contain crucial information on the shape, size, area, and volume of objects. Various industries, including agriculture and fisheries, have effectively utilized volume estimating methods based on point clouds (Guevara et al., 2020).

Due to a better portrayal of the region encompassed in the group of points, the Delaunay triangulation and voxelization procedures outperform in estimating the outcomes. These strategies, however, have a greater computational cost because of their accuracy (Auat Cheein et al., 2015). To es-

timate volume, methods such as Delaunay triangulation and voxelization are used. It is important to consider both accuracy and computing costs when using these methods. Height grids are faster for computing height discrepancies, but accuracy depends on precise point acquisition (Bewley et al., 2011; Duff, 2000).

The Delaunay triangulation-based technique for volume computation, known as Delaunay triangulation-driven volume calculation (DTVC), differs from traditional approaches which computes the volume during the triangulation process rather than preserving Delaunay triangles. This method reduces both memory usage and processing time. Experimental findings demonstrate that DTVC achieves a satisfactory trade-off between precision and efficiency (Liu and Zheng, 2021).

In computer graphics, a voxel is an image that depicts a specific region that has been partitioned into a grid of cubes that are all the same size and uniformly spaced (Putman and Popescu, 2018).

The Convex Hull is another method that is popular technique for measuring volume from 3D point cloud points (see figure 2.4). The computational geometry community has extensively studied the convex hull problem, as evidenced by the works of Kim (2002), Graham and Frances Yao (1983), and Maus (1984). Qhull is a commonly used algorithm to compute the convex hull, employing the Voronoi diagram, the Delaunay triangulation, furthest-site Voronoi diagram, the furthest-site Delauney triangulation,

and the half-space intersection around a point. The software program allows the creation of high-dimensional objects, and the Quickhull algorithm, written in C, is used to compute the convex hull, which solves round-off errors in floating-point arithmetic. The program is capable of calculating volumes, surface areas, and convex hull approximations.

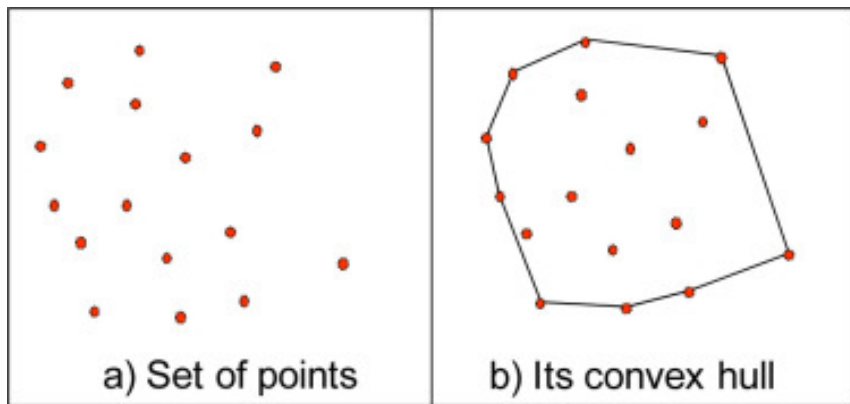


Figure 2.4. Convex Hull

Table 2.1 shows the percentage error analysis from the computed volume of different model point cloud objects in the study of Chang et al. (2017), which shows that in order to estimate the volume of a shape represented by a point cloud, the area of each slice of the shape is calculated by finding the difference between the top and bottom curves of the slice. The total volume of the shape is then calculated by integrating the areas of all the slices using an integration interval equal to the length of the point cloud.

Table 2.1. Point Cloud Volume of Different Model

Objects	True Value (mm ³)	Estimated Value (mm ³)	Error (%)
Cube	1 000 000	1 000 000	0
Cylinder	125.664	125.061	0.479
Sphere	4 188 90.2	4 178 966.87	0.234
Triangle Prism	17.321	17.399	0.45

The study conducted by Jeong et al. (2018) introduces a newly developed explicit hybrid numerical methodology for 3D volume reconstruction from unorganized point clouds, which is based on a modified Allen-Cahn equation and a 3D binary picture segmentation method. The technique has demonstrated potential in a variety of practical applications, including 3D model printing from dispersed scanned data. The computational findings show that the suggested approach for reconstructing 3D volume from point clouds is very efficient and resilient.

2.4 Robot Web Tools Application for ROS Remote Monitoring

The integration of Robot Web Tools (RWT) with ROS has garnered significant attention in recent years due to its potential to revolutionize real-time robotics applications. By leveraging web technologies and cloud computing infrastructure, developers aim to create intuitive interfaces for controlling and monitoring robots remotely. Central to the capabilities of RWT is its efficient messaging mechanism, which enables real-time interaction between web-based interfaces and ROS-enabled robots. By leveraging tech-

nologies such as roslibjs and rosbridge, RWT facilitates the seamless exchange of data, including sensor readings, point clouds, and control commands. This efficient messaging paradigm forms the backbone of RWT's ability to provide responsive and interactive interfaces for controlling and monitoring robotic systems.

Several studies have explored the capabilities of RWT in enabling real-time interaction with ROS-enabled robots. For instance, in a study by Qureshi et al. (2016), the development of a disaster management application is showcased, wherein Robot Web Tools (RWT) is utilized for seamless communication with ROS nodes. This integration enables an efficient response to emergencies by facilitating real-time interaction and control of robots remotely.

Furthermore, Lim (2019) explored the integration of ROS with cloud computing infrastructure to offload computationally intensive tasks and enhance scalability. They utilized RWT to develop web-based visualization tools for analyzing sensor data in real-time, showcasing its versatility in cloud robotics applications.

2.5 Synthesis of the Study

The conducted review of related literature provides a comprehensive overview of existing methods, techniques, and technologies used for volume measurement, point cloud acquisition devices, and volume measurement using 3D point cloud data. It highlights the importance of enhancing

post-harvest processing and storage technology to meet increasing global demand and minimize waste, emphasizing the role of advanced monitoring and management techniques in improving production efficiency and safety standards.

Various methods for volume measurement, including traditional level measurements and emerging technologies such as LiDAR, have been discussed. While traditional methods like weighted fiberglass tape provide a single data point, newer technologies offer more detailed and accurate measurements. Point cloud acquisition devices, particularly LiDAR, have emerged as powerful tools for generating detailed 3D models of objects or environments. Techniques for transforming 2D LiDAR scanners into 3D point cloud scanners have been explored, highlighting the use of rotating mechanisms and processing algorithms.

Additionally, the review discusses frameworks for point cloud processing, visualization, and mapping, emphasizing the importance of utilizing tools like ROS and PCL for efficient data handling. Techniques and methods for volume estimation using computational geometry, such as Delaunay triangulation and voxelization, have been examined, along with their applications in various industries.

Furthermore, the integration of Robot Web Tools (RWT) with ROS for remote monitoring of robots has been explored, demonstrating its potential in enabling real-time interaction and control of robots over the web. Several

studies have demonstrated the capabilities of RWT in disaster management, cloud robotics, and real-time sensor data analysis.

Given the advancements in point cloud acquisition devices, volume measurement techniques, and web-based robotics interfaces, this study focused on integrating and utilizing these technologies and methods to provide an alternative solution to existing technology used in storage volume calculation. By leveraging existing technologies and methodologies, the aim of this study was to develop a feasible approach for enhancing storage technology especially in volume measurement technology.

Table 2.2. Research Synthesis Matrix

Literature	Specific Objectives	Methodology	Problem: Unknown/Gap	Remarks
Kang et al. (2018)	To reconstruct complex 3D models using a low-cost 2D LiDAR by integrating an external rotary mechanism. The study sought to evaluate the feasibility and performance of this method in acquiring accurate 3D point cloud data.	The study used a 2D low-cost off-the-shelf LiDAR sensor combined with an external rotary mechanism to achieve 3D reconstruction. Experimental tests were conducted to assess the accuracy and effectiveness of this setup in 3D point cloud acquisition.	The research addressed the challenge of using low-cost 2D LiDAR sensors for 3D reconstruction, focusing on the increased complexity in hardware or software required for accurate 3D point cloud acquisition.	Concluded that integrating an external rotary mechanism allows low-cost 2D LiDAR sensors to perform 3D point cloud acquisition effectively. This approach increases system complexity but provides a cost-effective solution for 3D model reconstruction.
Yuan et al. (2021)	Aimed to create a 3D point cloud representation of the environment using a 2D LiDAR rotated by a stepper motor. The study focused on minimizing	The methodology involved rotating a 2D LiDAR using a stepper motor with the initial motor shaft position defined by photoelectric switches and	The research tackled the challenge of synchronizing a 2D LiDAR with a stepper motor for 3D point cloud creation without an absolute angle	Demonstrated that a 2D LiDAR, when rotated by a stepper motor and properly calibrated, can effectively generate a 3D point

Table 2.2 (contd.)

		<p>costs by employing a stepper motor and ensuring accurate system calibration to address errors from the lack of an absolute angle position.</p> <p>shading sheets. Intensive calibration was conducted to correct system errors by synchronizing the 2D LiDAR with the stepper motor, ensuring accurate 3D point cloud acquisition.</p>	<p>position. The focus was on developing a cost-effective yet precise solution for 3D data acquisition.</p>	<p>representation. The use of photoelectric switches and shading sheets for initial position definition and intensive calibration ensures system accuracy, providing a low-cost solution for 3D environment modeling.</p>
Clar and Salaan (2022)	Aimed to develop a more accurate and efficient method for estimating the volume of raw materials in silos using 3D mapping with point cloud processing.	The study used a 2D LiDAR scanner to scan a prototype silo, processed the data with ROS, and converted 2D scans to 3D using an algorithm. Outliers were removed statistically, and the Convex Hull method calculated the volume.	The research addressed the challenge of accurately estimating silo volumes due to uneven surfaces, which conventional methods struggle with. It highlighted the need for a more precise, efficient, and scalable solution.	Showed that the proposed method significantly improved volume estimation accuracy, however, The study conducted in a laboratory test and needs for large scale and a more compact and portable solution for larger-scale applications.

Table 2.2 (contd.)

Kim (2002)	Aimed to explore and address the convex hull problem in computational geometry, focusing on developing efficient algorithms for its computation.	Utilized various techniques, including the Voronoi diagram, Delaunay triangulation, furthest-site Voronoi diagram, furthest-site Delaunay triangulation, and half-space intersection around a point.	The research addressed the challenges of accurately computing convex hulls in high-dimensional spaces and resolving issues related to round-off errors in floating-point calculations.	The studies demonstrated that the Qhull program is effective in computing convex hulls, calculating volumes, surface areas, and providing convex hull approximations.
Jeong et al. (2018)	Aimed to develop an explicit hybrid numerical methodology for 3D volume reconstruction from unorganized point clouds, utilizing a modified Allen-Cahn equation and a 3D binary picture segmentation method.	The study introduced a novel technique combining the modified Allen-Cahn equation with 3D binary picture segmentation for reconstructing 3D volumes from unorganized point clouds.	The research addressed the challenge of efficiently reconstructing 3D volumes, a process essential for various practical applications but often hampered by inefficiencies and lack of robustness in existing methods.	Demonstrated that the proposed hybrid numerical methodology is both efficient and resilient, making it highly suitable for practical applications like 3D model printing from scanned data.

CHAPTER III

METHODOLOGY

In this chapter, the systematic approach for developing the proposed system is discussed. Figure 3.1 shows the system architecture, comprising a 3D point cloud scanner with a 2D LiDAR sensor, single board computer, and servo motor, all powered by a battery regulated with a buck converter. The flow chart in Figure 3.2 outlines the development process of the Web-based 3D Point Cloud Scanner System and Web Application, each phase is essential in shaping the overall system's functionality.

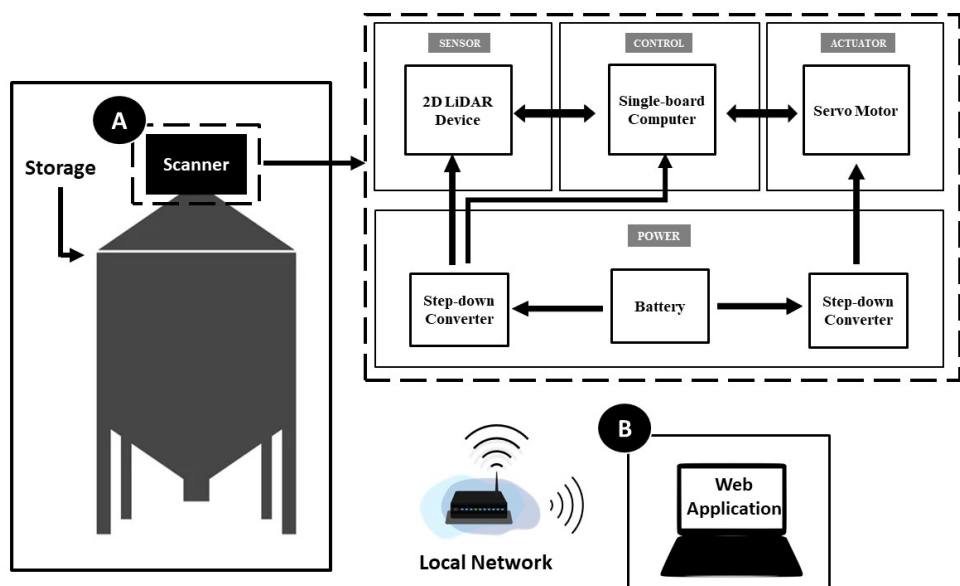


Figure 3.1. System Architecture Block Diagram: (A) 3D Point Cloud Scanner System, (B) Web Application

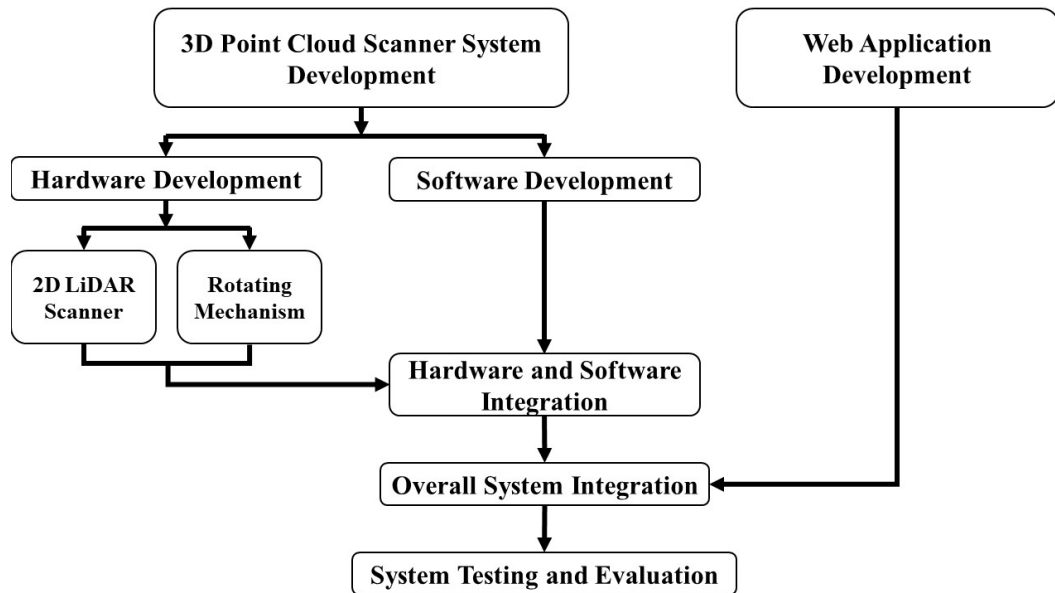


Figure 3.2. System Development Process

3.1 3D Point Cloud Scanner System Development

The development flow chart of the system is shown in figure 3.3 which composed of hardware and software development.

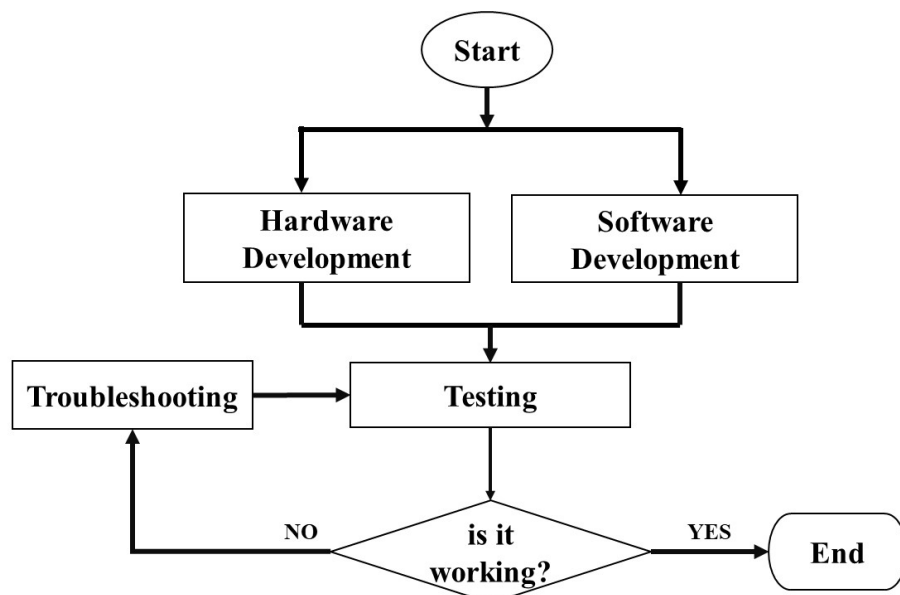


Figure 3.3. 3D Point Cloud Scanner Development Flow Chart

3.1.1 Hardware Development

The hardware components of the 3D Point Cloud Scanner System composed 2D LiDAR device and rotating mechanism.

3.1.1.1 2D LiDAR Scanner

The 2D LiDAR scanner comprises two major components: the 2D LiDAR Device and the single-board computer. The analysis of the hardware system requirements of 2D LiDAR Scanner in this study considers the following functionality:

- A 2D LiDAR device capable of scanning within a 180-degree horizontal field of view.

- A 2D LiDAR device with a minimum range measurement capability of 10 meters.
- A single-board computer with a minimum CPU speed of 1.8GHz (64-bit architecture), 4GB of RAM, 5GB of disk space, and compatible with the required operating system.

3.1.1.2 Rotating Mechanism

The rotating mechanism design which is attached to the 2D LiDAR in this study is based on the methodology outlined in a previous research conducted by Clar and Salaan (2022). This prior study served as a foundational framework for the development of the rotating 2D LiDAR system in this study, providing into the integration of a pan-tilt unit (PTU) with a 2D LiDAR scanner to enable three-dimensional point cloud scanning.

The functionality of the rotating device consider in this study has the following functionality:

- The rotating device can rotate a minimum angle from 0 of 180 degree.
- The rotating device has a minimum angular resolution of ≤ 1 degree.

Figure 3.4 provides an illustration of the servo's attachment to the 2D LiDAR device, enabling an additional axis of movement. It also demonstrates the respective scan angle directions of the LiDAR and the

movement direction of the servo motor. This synchronization method is further detailed in flow chart shown in Figure 3.5. After the LiDAR scans from 0 to 180 degrees, the system sends a command to the servo to move to the next angle until it reaches the end angle.

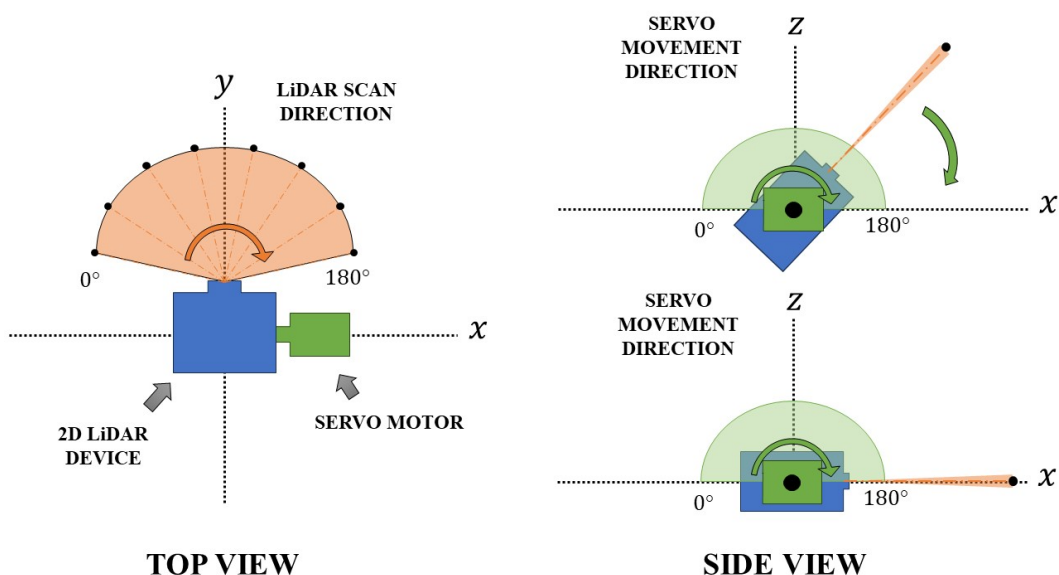


Figure 3.4. Scan Direction of LiDAR and Movement Direction of the Servo

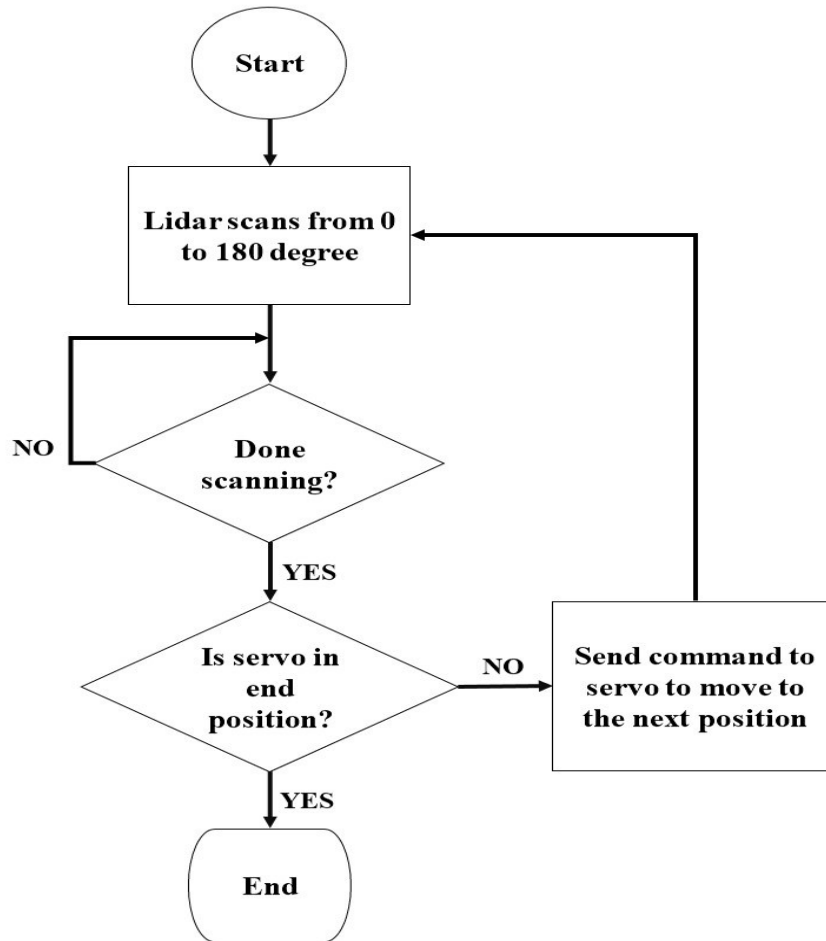


Figure 3.5. Synchronization Process of LiDAR and Servo

3.1.2 Software Development

Software development plays a crucial role in the overall development of the 3D Point Cloud Scanner System. The flow of the different software processes developed in this study is shown in figure 3.7. The system was designed to initialize all necessary components, including nodes and connection, immediately upon power-up. This ensures seamless operation and also establish connection with the developed web application for user inter-

action. Figure 3.6 shows the different nodes, topics and their relationship of the software of the system.

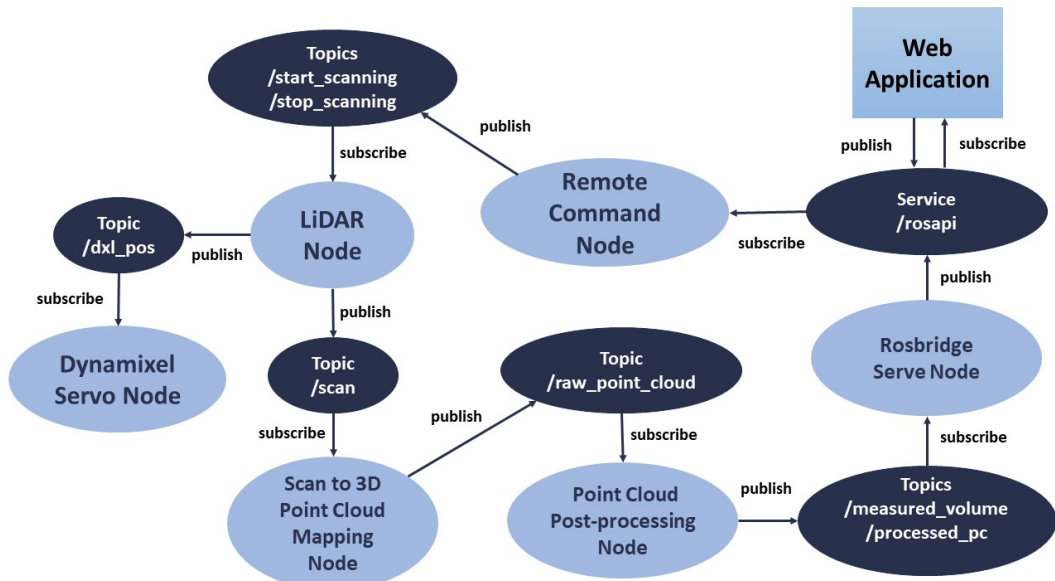


Figure 3.6. Nodes, Topics and their Relationships

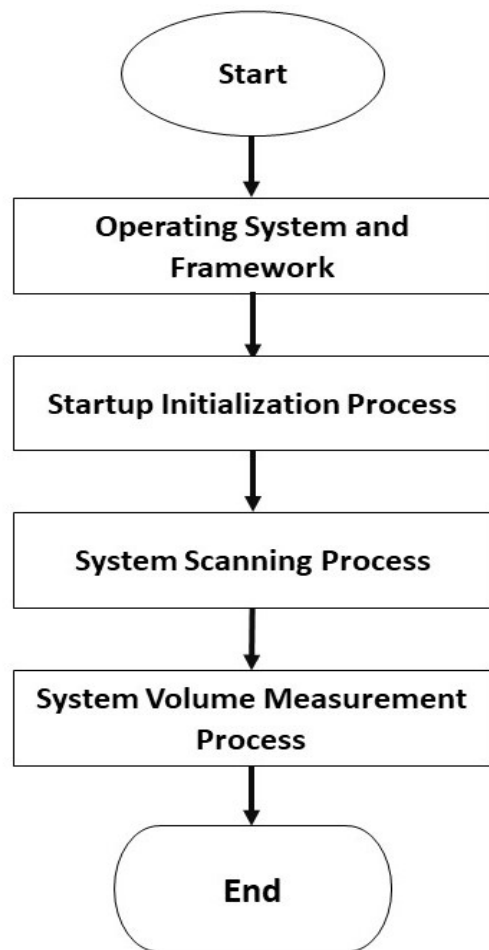


Figure 3.7. Flow Chart of the Different Software Processes

3.1.2.1 Operating System and Frameworks

In this study, the single-board computer (SBC) used in the 3D Point Cloud Scanner System requires an appropriate OS and frameworks to support the execution of firmware and software components. Linux-based operating systems, such as Ubuntu, is commonly chosen for SBCs due to its reliability, flexibility, and extensive community support. This OS option provide a stable platform for running Robot Operating Sys-

tem (ROS) nodes and managing system resources effectively, thus, was utilized in this study. ROS framework was also utilized in this study to develop a publish-subscribe relationship between ROS nodes. Lastly, Point Cloud Library (PCL) serves in this study as a fundamental library being used for processing and analyzing point cloud data. PCL provides a comprehensive set of algorithms and tools for tasks such as point cloud registration, filtering and computational geometry to name a few.

3.1.2.2 Startup Initialization Process

Roscore and rosbridge are the two essential cores that used in the software of 3D-PCSS. These cores typically need to be executed manually through the command-line interface (CLI) or desktop environment terminal to run and process data, or to initiate other nodes and do specific tasks. In this study a custom service file was developed to automate and start these nodes after the system is turn on. This file is created using Linux systemd to configure and instantly run the cores. As described in figure 3.8, after the system is energize, it initializes essential nodes and enter in idle mode waiting for an external command coming from the web application. The system remain in idle mode unless turnoff. The development of software processes, including the choice of operating system and frameworks is outlined in this section.

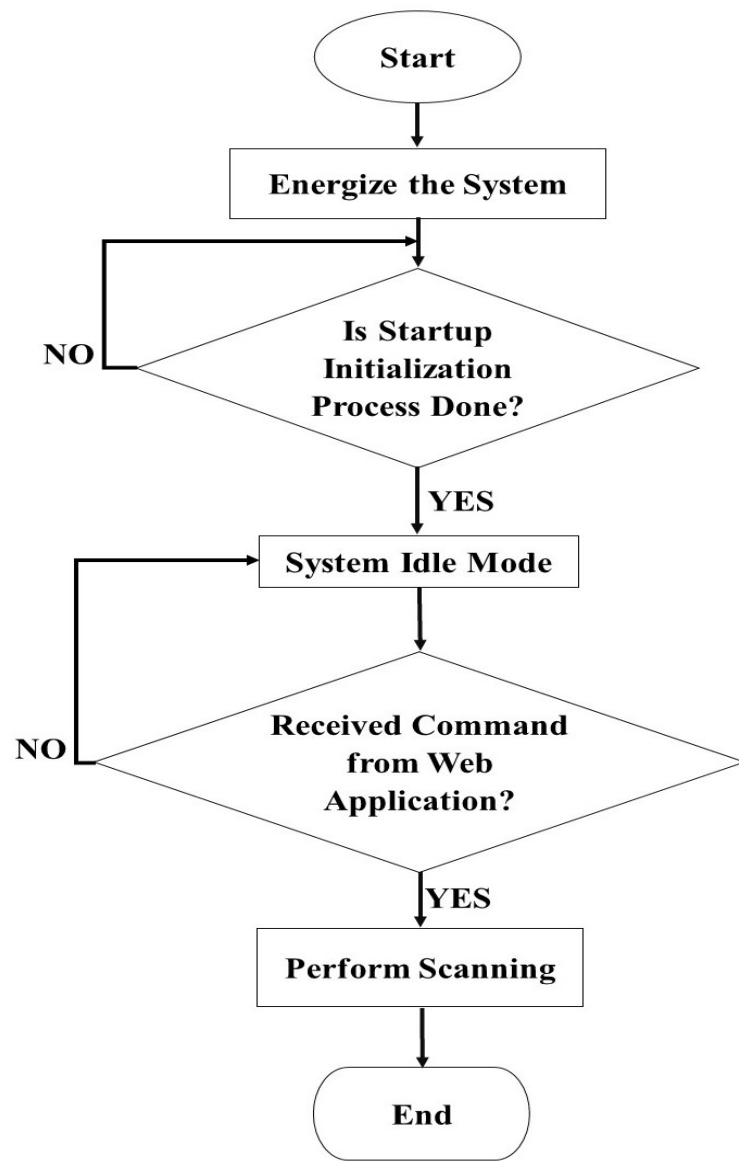


Figure 3.8. System Idle Mode Process Flow Chart

3.1.2.3 System Scanning Process

As described in conceptual framework shown in figure 1.1, the system is placed at the top of the storage bin. Once the system receive a command from the web application, it will start scanning the inside of

the storage bin and acquiring ranges values from the LiDAR as discussed in figure 3.8 else the system enters idle mode. The study developed a ros nodes that handle different processes such as initialization of the LiDAR device and servo motor, establishing a publish-subscribe relationship between these devices, and the conversion of LiDAR range scan data to point cloud data. The servo motor used in this study is compatible with a Software Development Kit (SDK) that includes configurations for integration with the Robot Operating System (ROS). The raw scan data from the LiDAR are typically range values of the return pulses. These range values enters different stages of pre-processes to be mapped in two- or three-dimensional Euclidean space to create a point cloud data and use for further post-processing. The flow of the processes from initialization to mapped point cloud data is illustrated in this figure 3.9. The method used in this study for processing the ranges values gathered from the LiDAR device is described in the figure 1.2 which was discussed in the theoretical framework. ρ translates to the distance from the origin $(0,0,0)$, which is the in our case the LiDAR, and this distance is measured as meter. The angle θ is the rotation around the z-axis in the xy-plane. The angle ϕ is the tilt of the radius vector from the positive z-axis, it goes from 0 degree at the positive z-axis down to 90 degree at the xy-plane and all the way down to 180 degree on the negative z-axis. Equation 3.1, 3.2 and 3.3 shows the X, Y, and Z conversion formula respectively.

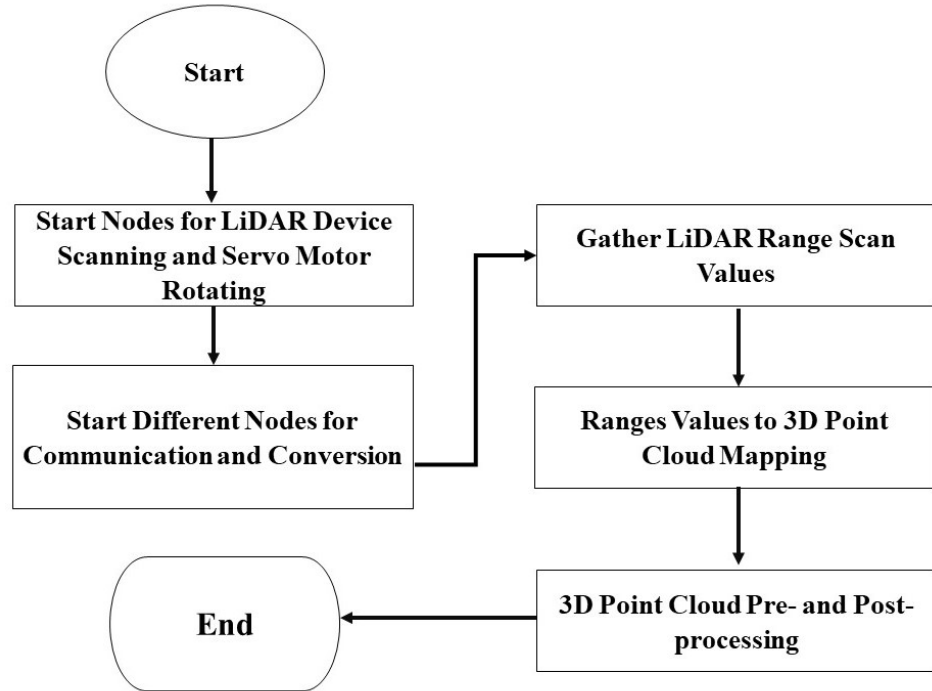


Figure 3.9. From Scanning to Mapped Point Cloud Data Flow Chart

$$x = \rho \cdot \sin(\theta) \cdot \cos(\phi) \quad (3.1)$$

$$y = \rho \cdot \sin(\theta) \cdot \sin(\phi) \quad (3.2)$$

$$z = \rho \cdot \cos(\theta) \quad (3.3)$$

3.1.2.4 Volume Measurement Process

An empty-space approach was used to measure the flour materials inside the storage bin. A simple representation of an empty-space approach is done following the concept discussed in section 1.7 where the 3D point cloud scanner system is placed at the top of the storage

bin to scan the empty space and generate point cloud data. These point cloud data are processed to calculate the empty space volume using the Convex Hull method, specifically utilizing the Quickhull algorithm. The Quickhull algorithm computes the convex hull of the gathered point cloud data, enabling for volume estimation. Theoretically, as shown in equation 3.4, the volume of the flour materials is determined by subtracting the empty space volume from the bin's maximum volume capacity, a commonly used method in these studies Raba et al. (2020); Clar and Salaan (2022).

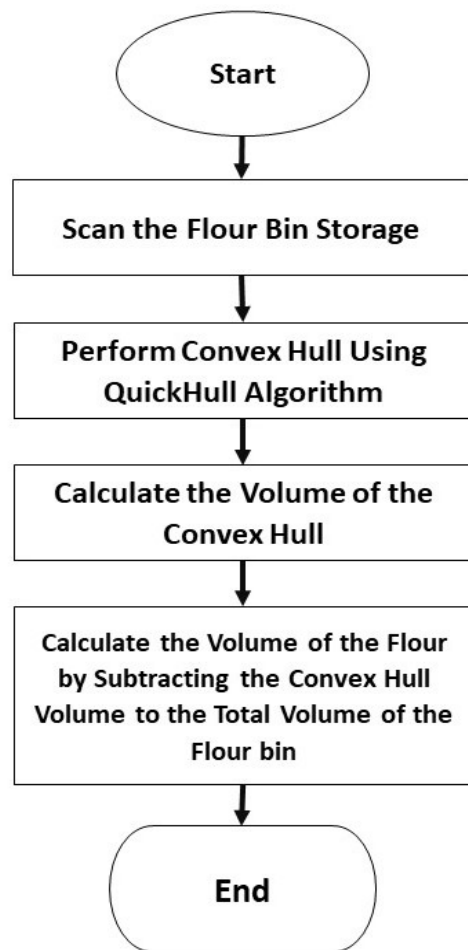


Figure 3.10. Flow Chart of the System's Volume Measurement Process

$$V_f = V_{max} - V_{empty} \quad (3.4)$$

Where:

V_f : Volume of the flour materials

V_{\max} : Total volume of the flour bin

V_{empty} : Volume of the empty space

3.2 Web Application Development

This section covers the process of developing the custom web application for the 3D point cloud scanner system.

3.2.1 Different Tools and Framework

The developed web application includes identifying the necessary tools and framework. These different tools and framework are essential for building the design and functionality of the UI. Table 3.1 outlines the various tools, frameworks, and libraries utilized in the implementation of the web application.

Table 3.1. Tools and Frameworks Used in the Web Application

Tool/Framework	Description/Functionality
jQuery	Used for simplifying JavaScript programming and DOM manipulation, jQuery is included via CDN for easy integration.
Three.js	This JavaScript library is utilized for rendering 3D graphics in a web browser. It enables the display of the 3D point cloud viewer within the application.
EventEmitter2	EventEmitter2 is employed for implementing event-driven programming, allowing efficient communication between different components of the application.
roslib.js	roslib.js is utilized for connecting the web application to the Robot Operating System (ROS), enabling communication with ROS nodes and topics.
Bootstrap	The Bootstrap framework is employed for responsive design and styling of the user interface components. It ensures consistency and enhances the visual appeal of the application.
Chart.js	This JavaScript library is used for creating interactive charts and graphs to visualize data. It enhances the user experience by providing intuitive data representation.
ros3d.js	ros3d.js is utilized for integrating ROS visualization capabilities into the web application. It facilitates the display of ROS topics such as point clouds and robot models.

These tools and frameworks collectively contribute to the functionality of the web application for the 3D Point Cloud Scanner System.

3.2.2 Dashboard Development

Analysis of the data and values to be displayed in the web application is conducted. This data and values are displayed in different section of the developed dashboard. The Web Application include storing of the measured volume coming from the system. The specific database used is MySQL which is running locally and retrieved to display in the dashboard.

3.2.3 Overall System Integration

Figure 3.11 shows the process flow chart of the scanner system and web app. The flow illustrates the different processes, starting from powering the system, up to saving the measured volume to the database.

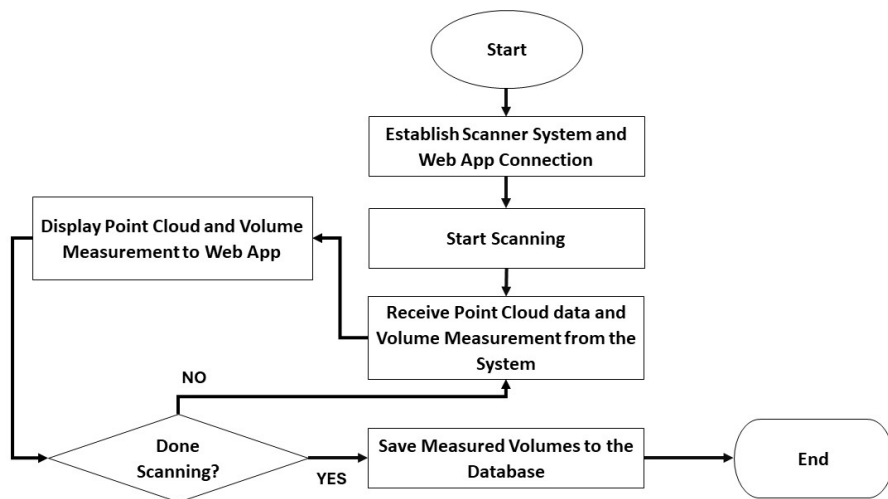


Figure 3.11. Process Flow Chart of Scanner System and Web App

The connection between scanner system and web application uses a

WebSocket communication protocol. This communication uses full-duplex channels to establish over a single TCP connection. It allows for less latency than typical HTTP connections when a client and server interact. Within the framework of ROS applications, WebSocket enables bi-directional, real-time communication, enabling servers to rapidly transmit updates to clients. The figure 3.12 demonstrate the initialization of the Websocket communication between the web interface and the 3D-PCSS. The following step to establish this communication is explain below:

1. **The Client Makes a Request:** The WebSocket client initiates the handshake by sending an connection request to the server.
2. **The Server Accepts the Request:** If the server is willing to establish a WebSocket connection, it responds with an accept response that has a status code of 101 (Switching Protocols).
3. **WebSocket Connection Established:** Once both the client and server have exchanged their handshake messages, the WebSocket connection is established. Data can now flow bidirectionally between the client and server over the single TCP connection.

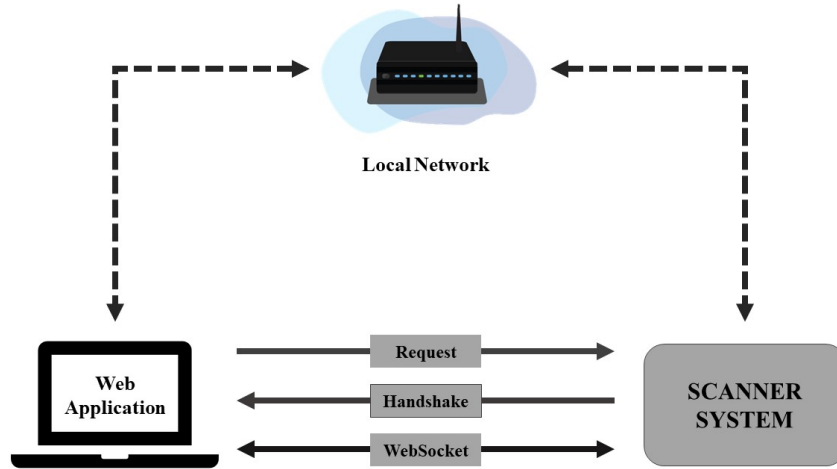


Figure 3.12. Communication Protocol of the Web Interface and the System

3.3 System Testing and Evaluation

The study conducted different tests and evaluation to observe the accuracy and performance of the overall system. The testing methods involved calibration test and volume measurement test of the system.

3.3.1 LiDAR and Servo Calibration Test

The purpose of the LiDAR and servo calibration test was to adjust the accuracy of the range values recorded and the rotating angle of the servo motor, which is crucial for ensuring that the system accurately captures the spatial data necessary for generating precise 3D point clouds. The calibration testing setup was done in the laboratory room, where the range values of the LiDAR device were calibrated using a known reference distance. The

LiDAR was positioned at various distances from the reference object, and the measured range values were compared against the known distances. Similarly, the angle of rotation of the servo motor was calibrated to ensure accurate positioning by commanding the servo to specific angles and verifying its actual position using a calibration tool, with any discrepancies between commanded and actual angles corrected through calibration adjustments.

3.3.2 System Volume Measurement Calibration Test

The calibration test aimed to assess the accuracy and reliability of the 3D Point Cloud Scanner System in measuring volume. This involved conducting various tests to evaluate the system's performance across different scenarios.

3.3.2.1 Testing Setup

The calibration test setup involved constructing a mock-up flour storage bin designed to closely mimic the geometric shape of the flour storage bins used in the industry. The CAD model design, shown in Figure 3.13, served as the guide for the physical construction. The design consisted of a rectangular shape with a conical frustum underneath.

The CAD design of the rectangular shape had the following dimensions:

- Height: 2.5 meters
- Length: 0.5 meters
- Width: 0.69 meters

The conical frustum, which tapers from the base of the rectangular section, had the following dimensions:

- Top radius: 0.21 meters
- Bottom radius: 0.17 meters
- Height: 0.42 meters

Before conducting different calibration test procedures, the system was calibrated and adjusted to minimize the error.

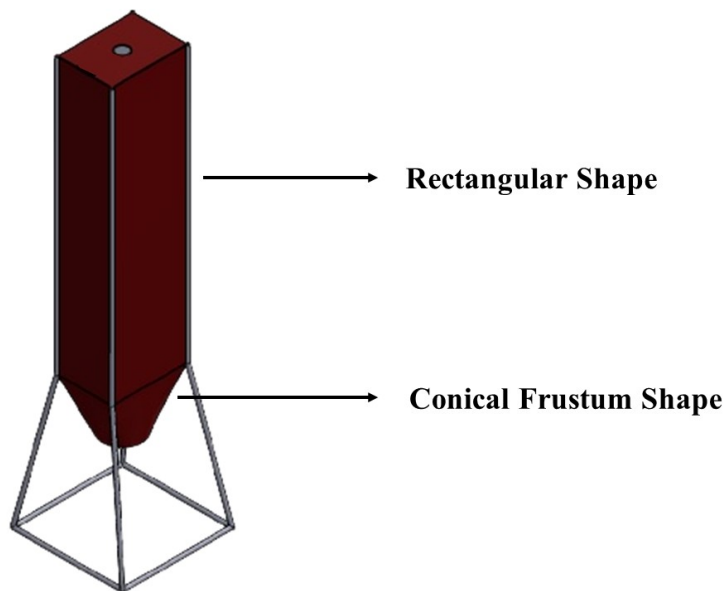


Figure 3.13. CAD Model Design of the Storage Bin

3.3.2.2 Empty Storage Volume Measurement Calibration

This calibration test involved performing multiple scans of an empty storage bin to measure its total volume. The purpose of this test was to scan the storage bin without any flour materials inside, ensuring an accurate baseline measurement. A total of 30 or more scanning trials were conducted. Before starting the test, the actual total volume of the flour storage bin was manually measured and calculated based on its geometric shapes and dimensions using a measuring tool like a steel tape measure.

3.3.2.3 Different Volume Quantity Measurement Calibration

This calibration test involved filling the storage bin with different quantities of flour materials to assess the system's accuracy in measuring varying volumes. A container with a known volume was used to ensure precise quantification of the added flour for comparison with the system's measurements.

Three specific volumes of flour were tested:

1. The storage bin was filled with $0.0594\ m^3$ of flour.
2. The storage bin was filled with $0.4752\ m^3$ of flour.
3. The storage bin was filled with $0.7128\ m^3$ of flour.

To test the consistency of the system, each volume test included two

different flour surface contours, with 5 multiple scans for each contour, totaling 10 scans per test scenario.

3.3.2.4 Volume Measurement Using the System and Sounding Method Test

To validate the accuracy and reliability of the 3D Point Cloud Scanner System, its volume measurements were compared with those obtained using the traditional sounding method. The traditional sounding method involves manually measuring the depth of the flour in the storage bin using a measuring tools such as tape measurement and calculating the volume based on the geometric shape and dimensions of the bin.

The comparison was conducted by filling the storage bin with a known volume of flour and measuring the volume using both methods. The specific steps were as follows:

1. The storage bin was filled with a known volume of flour.
2. The surface contour of the flour was adjusted into five different shapes.
3. For each contour shape, the volume was measured using the system and traditional sounding method.
4. The volume was then calculated based on the geometric shape and dimensions of the storage bin.

5. The results from both methods were recorded and compared.

3.3.3 System Evaluation

The system evaluation phase aimed to assess the overall performance and effectiveness of the system in fulfilling its intended objectives. This evaluation involved analyzing various aspects of the system, including the performance of the LiDAR sensor, the accuracy of servo motor control, and the reliability of volume measurement calculations.

3.3.3.1 LiDAR Range Evaluation

After the calibration of the device, any discrepancies or deviations from expected values are analyzed to identify and adjust. Performance assessment of LiDAR range involves conducting range measurements across different distances. The measured range values are compared against reference distances to evaluate accuracy and precision. The lidar range parameter is distances in meters,

3.3.3.2 Servo Angle Evaluation

The commanded and actual angles are compared to determine positional accuracy and repeatability. Additionally, the system's responsiveness to servo control commands is evaluated to assess its overall performance in angle adjustment and positioning tasks. The servo angle parameter

in degree.

3.3.3.3 Empty Storage Bin Volume Measurement Evaluation

In the evaluation of the Empty Storage Bin Volume Measurement test, the performance and accuracy of the system were assessed using several metrics. Firstly, the Mean Absolute Percentage Error (MAPE) was calculated by comparing the system's measured volume with the actual total volume of the storage bin. The average measured volume of the system was determined, considering the associated uncertainty. Lastly, the precision of the system was evaluated based on the closeness of the measured data points.

3.3.3.4 Different Volume Quatity Measurement Evaluation

In the evaluation of the Different Volume Measurement Test, the performance of the system in accurately measuring flour volumes of varying quantities was assessed using multiple evaluation metrics. The average measured volume with uncertainty was calculated for each test scenario. Moreover, the Mean Absolute Error (MAE) was used to evaluate the accuracy of the system's measurements across the different volume quantities. Lastly, the performance of the system in terms of precision across the different volume quantity was assessed.

3.3.3.5 Comparison Evaluation of the System and Sounding Method

In this comparison evaluation, the system's volume measurements were compared with those obtained using the traditional sounding method. A known volume of flour was filled into the storage bin, and the surface contour was adjusted into five different shapes. For each contour shape, volume measurements were taken using both the 3D Point Cloud Scanner System and the traditional sounding method. The accuracy and reliability of the system were evaluated by comparing the measured volumes from both methods and calculating the percentage differences. This comparison aimed to highlight the system's overall performance over sounding method.

CHAPTER IV

RESULT AND DISCUSSION

The results of the system development outlined in the previous chapter were presented and discussed in this chapter. After evaluating the specification of each system and undergo different design revision and integration, the study successfully identified and finalized the necessary components, tools and materials for each system.

4.1 3D Point Cloud Scanner System

The CAD Design of 3D Point Cloud Scanner System setup, as shown in figure 4.1, consists of a 2D LiDAR Device fixed to a platform connected to a servo motor. This servo motor allows the platform to rotate, giving the LiDAR device an extra axis of movement. The 2D LiDAR device and servo motor used in this study are the YDLiDAR X4 Model and AX12A Dynamixel servo motor respectively. The detailed specification of each of the components is presented in appendix A.

Inside the compartment is where the single-board computer along with other circuit components located. The system is powered by a battery Inside the compartment, the specific components and its category is shown in figure 4.2 and the system is powered by a battery.

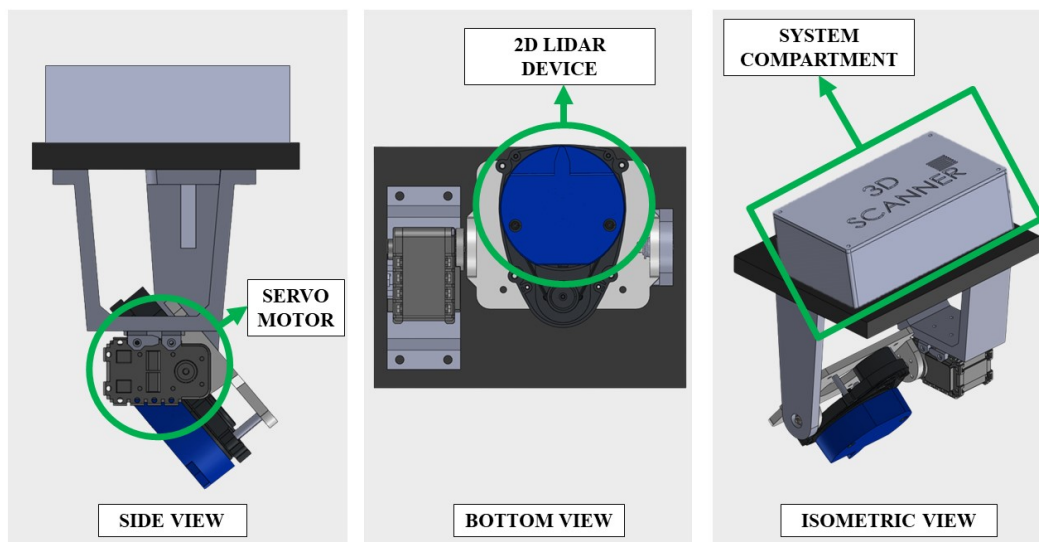


Figure 4.1. Different View of the CAD Model Design of 3D Point Cloud Scanner System

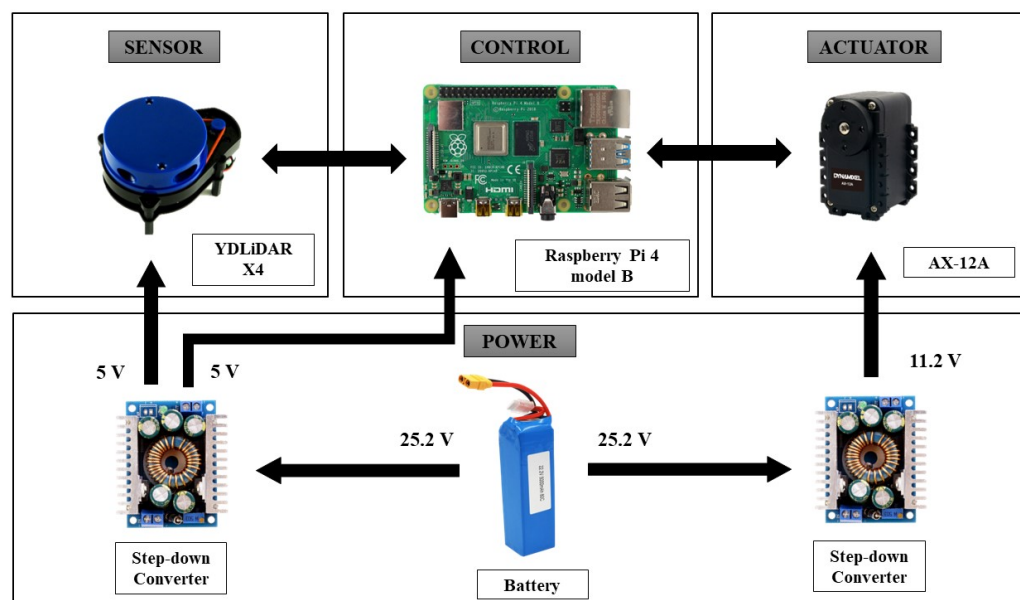


Figure 4.2. Specific Components of the System

4.1.1 Actual Prototype of the 3D Point Cloud Scanner System

The actual 3D Point Cloud Scanner System developed is shown in figure 4.3 was constructed in accordance with the 3D CAD model design. Before the integration of the system, individual component testing were conducted to test and verify if such components function properly. The base platform, to which the 2D LiDAR device and servo motor are attached, was fabricated using aluminum metal. The system compartment was 3D printed. Figure 4.4 shows the circuit diagram of the system.



Figure 4.3. Actual 3D Point Cloud Scanner System Developed

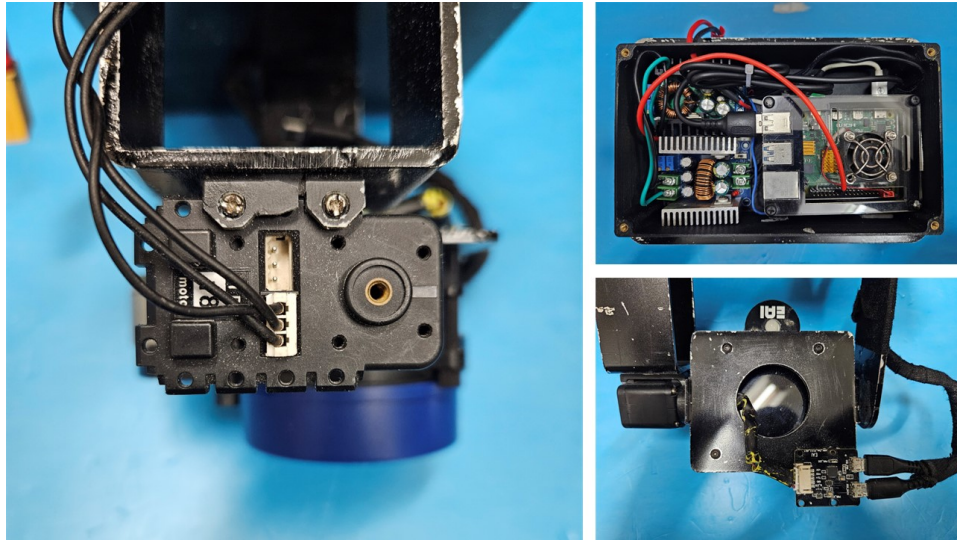


Figure 4.4. Actual Circuit Components of the System

4.1.2 Software Development Result

The processes of the system discussed in section 3.1.2 were implemented on the single-board computer (Raspberry Pi 4 model B), which serves as the central component driving the functionality of the 3D Point Cloud Scanner System.

The figure 3.6 demonstrated in chapter 3 illustrates the developed processes of the system, structured around a publish-subscribe model, facilitating efficient communication and data exchange between different nodes. The arrows in the diagram show how data flows between the different nodes and its relationship to a corresponding topics. The ROS bridge server Node facilitates communication by relaying commands between the web application and the ROS framework via the `/rosapi` service. Commands to start

and stop scanning from the web interface are processed using the Remote Command Node within the system. The LiDAR Node captures ranges data and publishes it as distance values (meter), while the Dynamixel Node and LiDAR Node synchronize their operations through the `/dxl_pos` topic. The Scan to 3D Point Cloud Mapping Node converts raw scan data into usable 3D point cloud data. The data type associated with the topics provided such as `/raw_point_cloud` and `/processed_pc` comprise a structured format, representing individual data points in three-dimensional space. Attributes within this data structure include spatial coordinates (e.g., X, Y, Z), intensity values, angles, and timestamps. The post-processing stage refines the point cloud data for volume measurement. Lastly, the expected value from the topic `/measured_volume` corresponds to the volumetric value expressed in cubic meters (m^3) which is from the calculated volume of Convex hull.

Figure 4.5 illustrates an example of the developed volume estimation process of the system. The raw data from the LiDAR is converted into point cloud data. This point cloud data can then use the convex hull to create a mesh for volume estimation. The Quickhull algorithm used for this process is shown algorithm 1.

Algorithm 1 Quickhull Algorithm for 3D Point Cloud Volume Calculation

Require: Point cloud data P

Ensure: Convex hull H and volume V

- 1: Initialize dimension $d = 3$
- 2: Allocate memory for coordinates of points in P
- 3: **for** each point p in P **do**
- 4: Store coordinates of p in array
- 5: **end for**
- 6: Initialize Quickhull with d and the array of points
- 7: Compute the convex hull using Quickhull
- 8: **if** Quickhull fails **then**
- 9: Output error and terminate
- 10: **end if**
- 11: Triangulate the convex hull
- 12: Extract the number of facets and vertices from the hull
- 13: Allocate memory for hull vertices
- 14: **for** each vertex in the hull **do**
- 15: Map Quickhull vertex ID to point cloud index
- 16: Add vertex to hull
- 17: **end for**
- 18: **if** area and volume computation is enabled **then**
- 19: Compute the total area and volume of the hull
- 20: **end if**
- 21: **if** polygon data filling is enabled **then**
- 22: **for** each facet in the hull **do**
- 23: Extract vertices of the facet
- 24: Store the facet vertices
- 25: **end for**
- 26: **end if**
- 27: Deallocate memory used by Quickhull
- 28: Output convex hull H and volume V

The algorithm handles the 3D point cloud data and perform convex hull and volume estimation as follow:

- **Initialize Dimension and Memory:**

- Set the dimension to 3 (for 3D).

- Allocate memory for the coordinates of the points in the point cloud.

- **Store Coordinates:**

- Loop through each point in the point cloud and store its coordinates in an array.

- **Initialize and Compute Convex Hull:**

- Initialize Quickhull with the dimension and the array of points.
- Compute the convex hull using Quickhull.

- **Error Handling:**

- If Quickhull fails to compute the hull, output an error message and terminate the algorithm.

- **Triangulate Convex Hull:**

- Triangulate the convex hull to facilitate volume computation.

- **Extract and Map Vertices:**

- Extract the number of facets and vertices from the hull.
- Allocate memory for the hull vertices.
- Loop through each vertex, map the Quickhull vertex ID to the point cloud index, and add the vertex to the hull.

- **Compute Area and Volume (if enabled):**

- Compute the total area and volume of the hull if area and volume computation are enabled.
- **Fill Polygon Data (if enabled):**
 - Loop through each facet in the hull, extract the vertices of the facet, and store them.
- **Deallocate Memory:**
 - Deallocate the memory used by Quickhull.
- **Output:**
 - Output the convex hull and its volume.

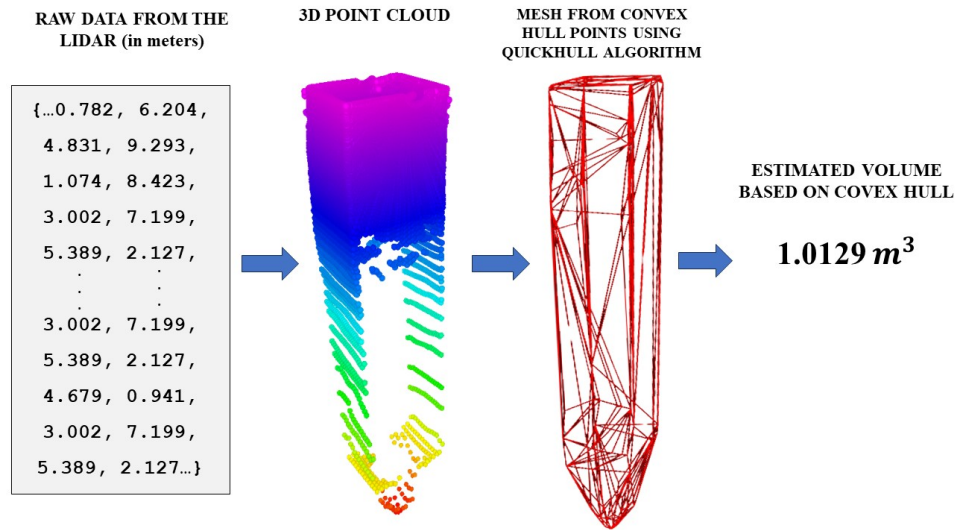


Figure 4.5. Example of the Volume Estimation Process of the System

4.2 Web Application Implementation

The implementation result of the analysis for developing the web application is discussed in this section.

The developed main dashboard of the UI, as shown in Figure 4.6, consists of three distinct sections. On the left side is the System Status section provides visual feedback regarding the establishment of the connection with the system, allowing users to monitor and verify the connection status. Additionally, users can access a list of currently active topics by clicking the List of Topics button. In the center section, users can visualize with the 3D point cloud data scanned from the system. This includes functionalities such as zooming in and out or moving the visualization. Moreover, in this section the start and stop scanning button is located, enabling users to send command to the system. Finally, on the right side, users can access volume measurement values and other numerical information, such as storage capacity. Users also have the option to input the known maximum volume capacity of the storage bin being used. The save button is also located in this section to store in the database the Empty Space Volume, Product Volume and the Percentage Capacity of the storage bin.

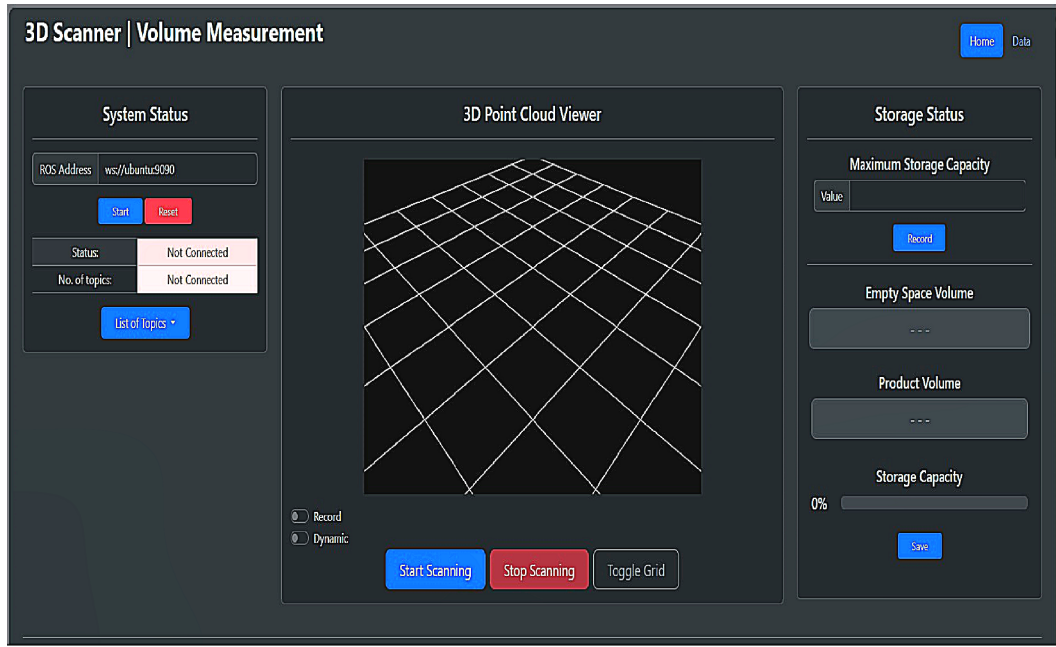


Figure 4.6. Main Dashboard

In the data section of the dashboard, users can visualize both the data table and the graph, as depicted in figures 4.7, respectively. This data was retrieved from the developed database that were running locally.

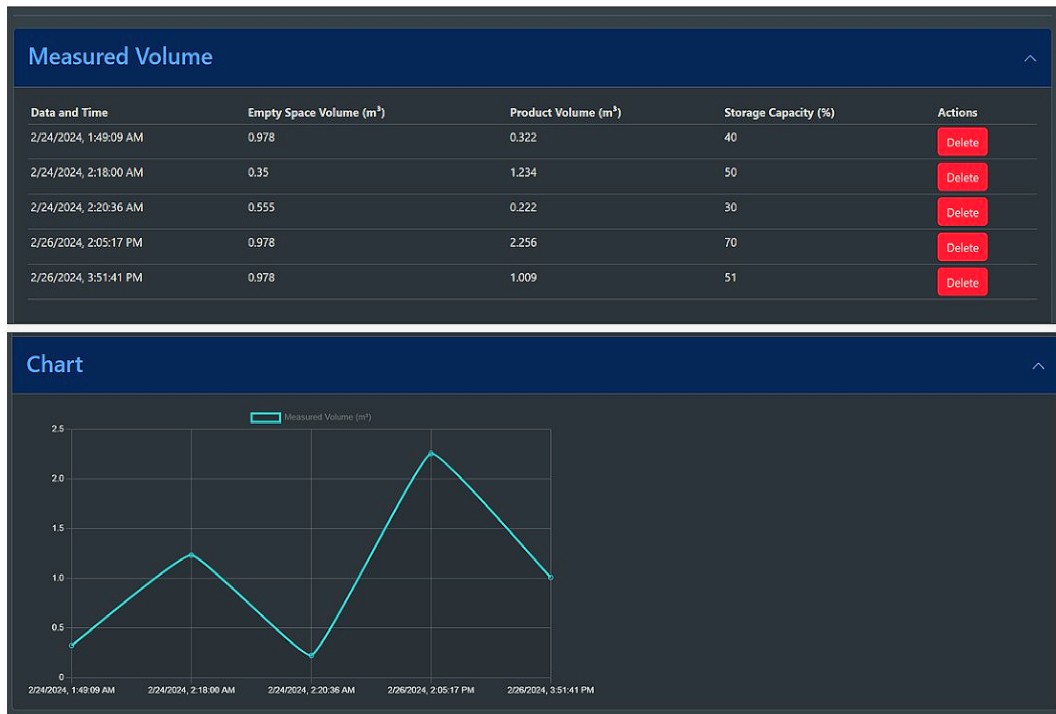


Figure 4.7. Data Section

The developed database was integrated to the web application, this database was running locally. Figure 4.8 shows the single database table schema. The table shows a unique identifier for each record (id), a date and time stamp (date), and float values for the empty space (empty_space_volume), product volume (product_volume) and int value for storage capacity (storage_capacity).

measured_volume	
PK	<u>id int NOT NULL</u>
	date_time datetime NOT NULL empty_space_volume float NOT NULL product_volume float NOT NULL storage_capacity int NOT NULL

Figure 4.8. Single Database Schema of the Web Application

4.2.1 Overall System Integration

The system and the Web interface were integrated and test their functionalities. The connection between the system and the web application were verified. Both system are within the same local network and utilizes WebSocket communication protocol, this protocol were discussed in the section 3.2.3. After verifying the connection between the systems, further tests were conducted to ensure successful overall system integration.

4.3 System Testing and Evaluation Result

After conducting the various tests outlined in Section 3.3, the following result of each testing is discussed and evaluate in this section.

4.3.1 LiDAR and Servo Calibration Test Result

This section discusses the results of the calibration tests conducted to fine-tune the range measurement capabilities of the LiDAR sensor and the

rotational accuracy of the servo motor. The actual images of the calibration testing is shown in Appendix B.

4.3.1.1 LiDAR Range Calibration

Five trials were conducted, with the LiDAR sensor capturing range data for five different reference points. The results of the calibration test are summarized in Table 4.1.

Table 4.1. LiDAR Range Calibration Results

Actual Range (m)	Measured Range (m)					Average (m)
	Trial 1	Trial 2	Trial 3	Trial 4	Trial 5	
1	1.0134	1.0135	1.0367	1.0154	1.0135	1.0185
1.5	1.5267	1.5278	1.5165	1.5073	1.4975	1.51516
2	2.0289	2.0353	2.0145	2.0184	2.0095	2.02132
2.5	2.5241	2.5342	2.5092	2.5276	2.5502	2.52906
3	3.0412	3.0353	3.0452	3.0221	3.0317	3.0351

4.3.1.2 Servo Angle Calibration

The servo angle calibration test focused on assessing the rotational accuracy of the servo motor, which determines the orientation of the LiDAR sensor during scanning operations. Similar to the LiDAR range calibration, five trials were conducted to evaluate the servo's performance across various angular positions. The results of the calibration test are presented in Table 4.2.

Table 4.2. Sevo Angle Calibration Results

Actual Angle (°)	Measured Angle (°)					Average (°)
	Trial 1	Trial 2	Trial 3	Trial 4	Trial 5	
35	35	36	35	35	35	35.2
70	70	71	70	70	69	70
105	106	105	106	104	105	105.2
140	140	141	139	141	140	140.2
175	175	175	174	174	176	174.8

4.3.2 System Volume Measurement Calibration Result

The different volume measurement calibration testing outline in section 3.3.2 were conducted. The results of these testing are discussed further in this section, and the images of the actual testing conducted is shown in appendix B.

4.3.2.1 Testing Setup Result

The design specifications outlined of the proposed storage bin in section 3.3.2.1 were implemented to construct a mock-up storage bin. In the actual mock-up bin consists of three distinct geometric shapes as depicted in Figure 4.9. The dimensions of each shape were manually measured using a steel tape measure.

- The rectangular shape has the following dimension:

- Height: 2.775 meters

- Length: 0.5 meters
- Width: 0.69 meters
- The pyramidal frustum shape has the following dimensions:
 - Upper length: 0.5 meters
 - Upper width: 0.69 meters
 - Height: 0.03 meters
 - Lower length and width: 0.42 meters
- The conical frustum shape features the following dimensions:
 - Top radius: 0.21 meters
 - Bottom radius: 0.17 meters
 - Height: 0.42 meters

With these dimensions, the individual and total volume capacities of the storage bin were calculated. Table 4.3 provides a summary of the measured individual and total volume capacity of the bin.

Table 4.3. Individual and Total Volume of the Storage Bin

Shape	Actual Volume (m^3)
Rectangular	0.9573
Pyramidal Frustum	0.0077
Conical Frustum	0.0478088
Total	1.012875

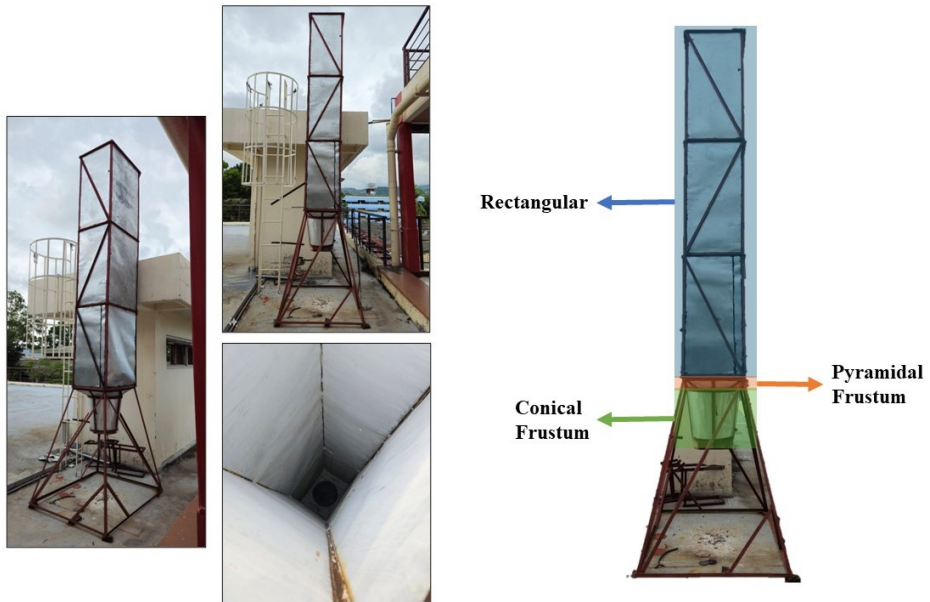


Figure 4.9. Actual Flour Storage Bin Created

The actual field system setup shown in figure 4.10 demonstrate the placement of the 3D Point Cloud Scanner System and the end-user device where the web application is running. The actual field of testing situated within the university premises.

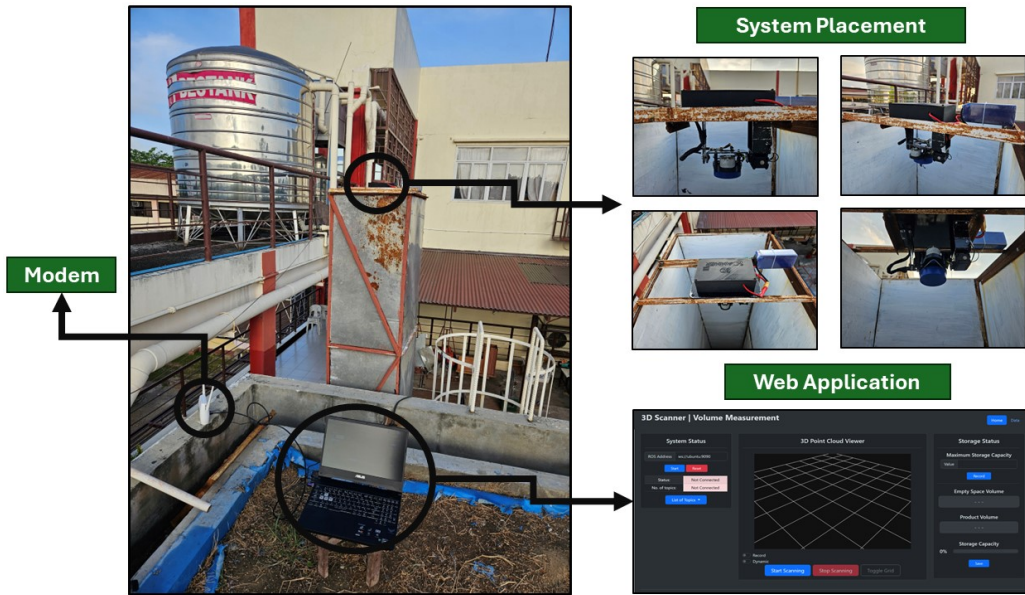


Figure 4.10. Testing Field and The Actual System Setup

4.3.2.2 Empty Storage Volume Measurement Calibration Test Result

Multiple scans and volume measurement of an empty storage bin were performed. Figure 4.11 shows the sample point cloud scan of the system and the actual empty bin. Table 4.4 presents the results obtained from 37 scanning trials. The actual visualization of the point cloud and volume are shown in figure 4.12.

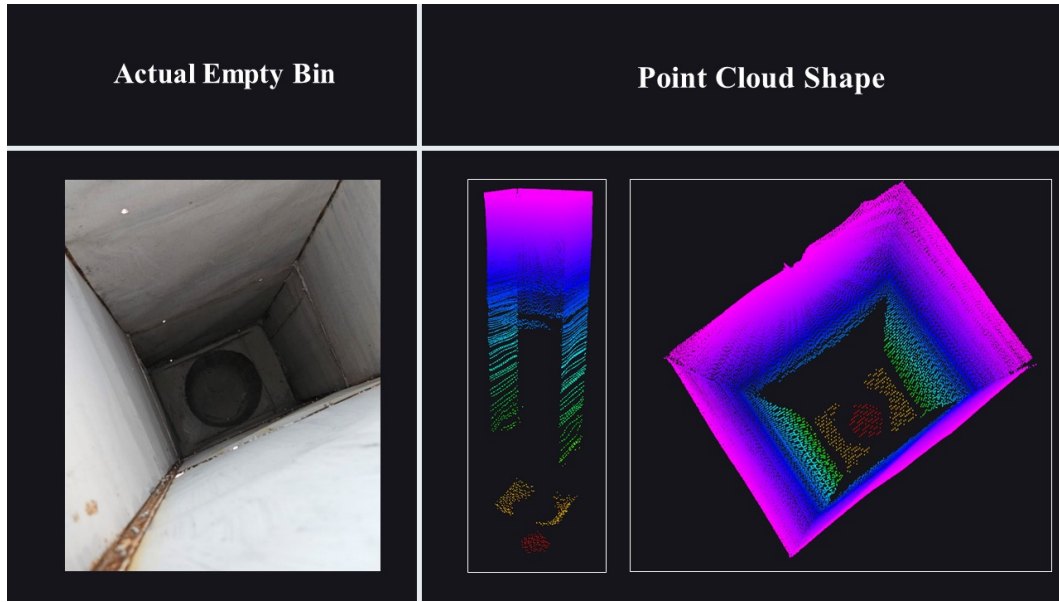


Figure 4.11. Actual Empty Bin and Scanned Point Cloud Data

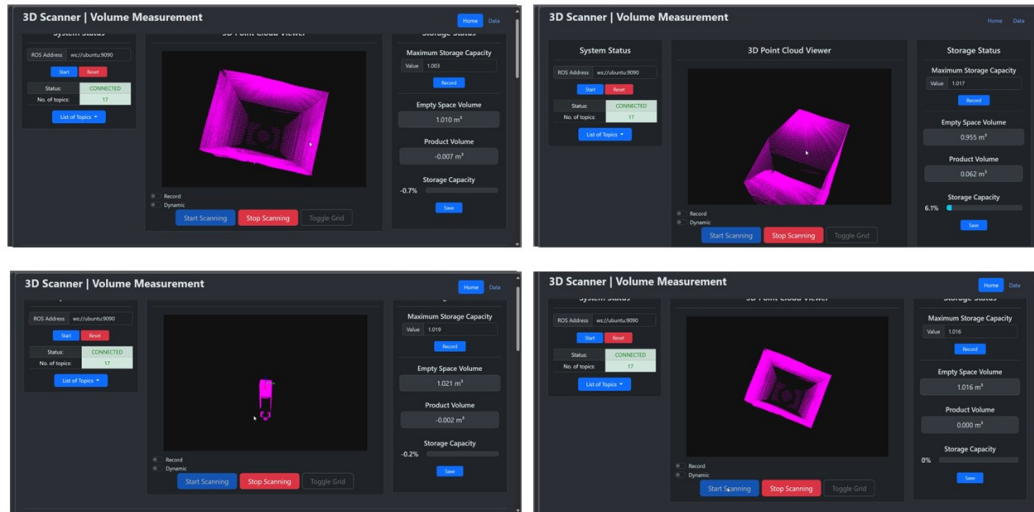


Figure 4.12. Actual Web Visualization of Point Cloud and Volume

Table 4.4. Actual and Measured Volume of Empty Storage Bin Volume Measurement Result

Trials	Measured Volume of the System (m^3)	Storage Actuatl Total Volume (m^3)
1	1.0118	1.0129
2	1.0120	1.0129
3	1.0120	1.0129
4	1.0130	1.0129
5	1.0123	1.0129
6	1.0130	1.0129
7	1.0110	1.0129
8	1.0110	1.0129
9	1.0112	1.0129
10	1.0123	1.0129
11	1.0120	1.0129
12	1.0120	1.0129
13	1.0110	1.0129
14	1.0190	1.0129
15	1.0110	1.0129
16	1.0130	1.0129
17	1.0140	1.0129
18	1.0120	1.0129
19	1.0110	1.0129
20	1.0100	1.0129
21	1.0130	1.0129
22	1.0160	1.0129
23	1.0140	1.0129
24	1.0140	1.0129
25	1.0160	1.0129
26	1.0150	1.0129
27	1.0110	1.0129
28	1.0110	1.0129
29	1.0110	1.0129
30	1.0160	1.0129
31	1.0170	1.0129
32	1.0127	1.0129
33	1.0120	1.0129
34	1.0123	1.0129
35	1.0110	1.0129
36	1.0130	1.0129
37	1.0130	1.0129

Based on the graph shown in figure ??, the average measured volume of the system is 1.0128 m^3 . The actual total volume of the storage bin is 1.0129 m^3 . To determine the actual volume of the storage bin, the study calculated the total volume it can store based on its dimensions and geometric volume.

To determine whether it is statistically different from the mean of the storage total volume of 1.0129 m^3 to the mean measured volume of the system, the study conducted a One-Sample t-test. According to the p.value which is above 0.05, there is no statistically significant difference detected.

4.3.2.3 Different Volume Quantity Measurement Calibration Test Result

In this test, three different scenarios were conducted as discussed in section 3.3.2.3, the flour storage bin was filled with different volume flour materials: **(1) 0.0594 m^3 , (2) 0.4752 m^3 and (3) 0.7128 m^3** . A container with a known volume was used throughout this test for filling the storage bin as shown in figure 4.13. This container was measured manually and has a total volume capacity of 0.0594 m^3 .



Figure 4.13. Container with a Known Volume Used for Testing

1. Storage Bin Filled with 0.0594 m^3 of Flour

Figure 4.14 illustrate the actual flour surface contours along with the point cloud shapes by the system. The measured volumes of the two contours and the distribution of the data is presents in table 4.5.

	Actual Shape	Point Cloud Shape
Contour 1		
Contour 2		

Figure 4.14. Actual and Point Cloud Surface Contour of Test 1

Table 4.5 presents the calibration result of the volume measure-

ment of the system, which compares the measured volumes of two contours against a known volume of 0.0594 m^3 across five trials. Contour 1 exhibited an average measured volume of 0.059678 m^3 , resulting in a slightly higher estimation of the actual volume. Conversely, Contour 2 demonstrated a closer correspondence with the known volume, with an average measurement of 0.0595 m^3 . Both contours displayed minimal deviations in measured volume across trials, suggesting reasonable accuracy and precision.

Table 4.5. Volume Measurements Calibration Result of the System Across Two Contours with A Known Volume of 0.0594 m^3

Trials	Measured Volume (m^3)		Known Volume (m^3)
	Contour 1	Contour 2	
1	0.06	0.0592	0.0594
2	0.05934	0.0601	0.0594
3	0.058943	0.0589	0.0594
4	0.05976	0.0591	0.0594
5	0.059678	0.0602	0.0594
Average	0.059678	0.0595	

Based on the conducted ANOVA test and the statistic analysis table can be seen in Appendix C table C.2, there is no statistical difference for the 0.0594 m^3 level volume measurement according to the actual volume and those with different contours measured by the system with p value greater than 0.05.

2. Storage Bin Filled with 0.4752 m^3 of Flour

A flour of 0.4752 m^3 was filled in the storage bin. Figure 4.15 illustrates the actual flour surface contours along with the scanned point cloud contour by the system. The measured volumes across the two contours and the distribution of the data are presented in table 4.6.

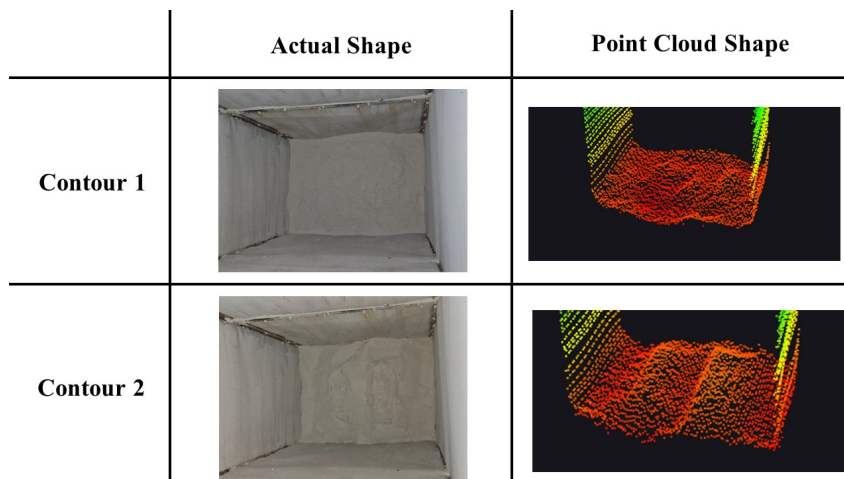


Figure 4.15. Actual and Point Cloud Surface Contours of Test 2

The table 4.6 presents the results of volume measurements calibration for a system across two contours, compared against a known volume of 0.4752 m^3 . Over five trials, Contour 1's measured volumes range from 0.470279 m^3 to 0.4805594 m^3 , with an average of 0.47407038 m^3 , slightly lower estimation to the actual volume. Contour 2's measurements range from 0.464461 m^3 to 0.485587 m^3 , with an average of 0.473391 m^3 , also slightly underestimating the actual volume. Both contours show minor variations, with Contour 1 being marginally closer

to the actual volume on average.

Table 4.6. Volume Measurements Calibration Result of the System Across Two Contours with A Known Volume of $0.4752\ m^3$

Trials	Measured Volume (m^3)		Known Volume (m^3)
	Contour 1	Contour 2	
1	0.470418	0.472914	0.4752
2	0.470279	0.464461	0.4752
3	0.472061	0.473782	0.4752
4	0.4805594	0.485587	0.4752
5	0.4770345	0.470211	0.4752
Average	0.47407038	0.473391	

Based on the conducted ANOVA test and the statistic analysis table can be seen in Appendix C table C.3, there is no statistical difference for the $0.4752\ m^3$ level volume measurement according to the actual volume and those with different contours measured by the system with p value greater than 0.05.

3. Storage Bin Filled with $0.7128\ m^3$ of Flour

A volume of $0.7128\ m^3$ was filled in the storage bin. Figure 4.16 illustrates the actual flour surface contours along with the scanned point cloud contour by the system. The measured volumes across the two contours and the distribution of the data are presented in table 4.6.

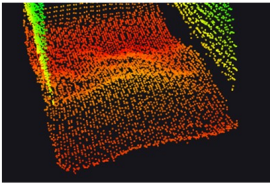
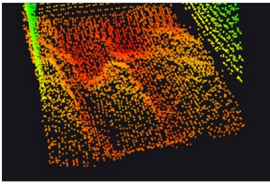
	Actual Shape	Point Cloud Shape
Contour 1		
Contour 2		

Figure 4.16. Actual and Point Cloud Surface Contour of Test 3

The table 4.7 presents the calibration results of volume measurements of the system across two contours, compared against a known volume of 0.7128 m^3 filled in the flour bin. Over five trials, Contour 1 gathered an average measured volume of 0.7178206 m^3 , slightly higher estimation to the known volume. The Contour 2 gathered an average measured volume of 0.7202706 m^3 , also slightly higher estimation to the known volume. Both contours show minor variations, with Contour 1 being marginally closer to the known volume on average.

Table 4.7. Volume Measurements Calibration Result of the System Across Two Contours with A Known Volume of $0.7128\ m^3$

Trials	Measured Volume (m^3)		Known Volume (m^3)
	Contour 1	Contour 2	
1	0.716327	0.725803	0.7128
2	0.706001	0.724873	0.7128
3	0.720251	0.729404	0.7128
4	0.71687	0.715844	0.7128
5	0.729654	0.705429	0.7128
Average	0.7178206	0.7202706	

Based on the conducted ANOVA test and the statistic analysis table can be seen in Appendix C table C.3, there is no statistical difference for the $0.7128\ m^3$ level volume measurement according to the actual volume and those with different contours measured by the system with p value greater than 0.05.

4.3.2.4 Volume Measurement Using the System and Sounding Method Result

The results of the comparison are summarized in table 4.8. The table presents the measured volumes using both methods for each contour shape and the percentage difference between them. The graph shown in 4.17 represents the distribution of volumes obtained from two different methods (system and sounding) for five contour trials. The actual testing images and scanned point cloud of the system can be seen in Appendix

B under System and Sounding Method Actual Testing section.

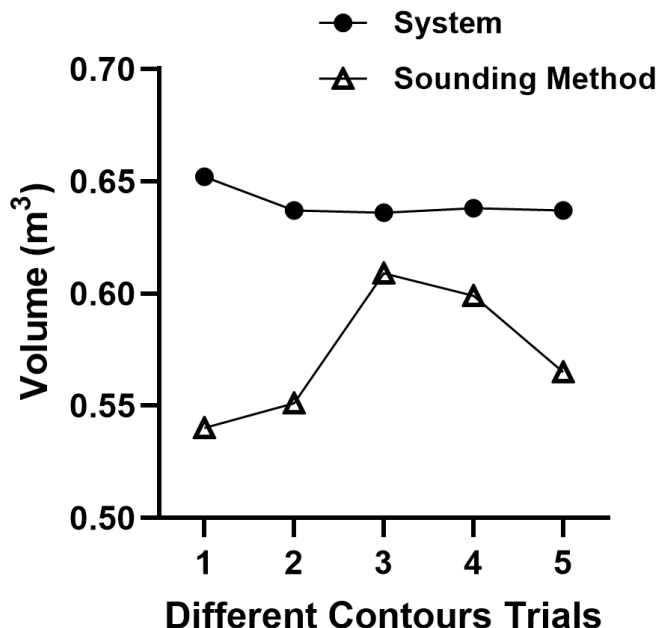


Figure 4.17. Distribution of volume measurements obtained from the system and sounding

The table 4.8 compares volume measurements using the system and the traditional sounding method against an actual volume of 0.639 m^3 across five trials each trials changed the contour surface of the flour. The measured volumes using the scanner system range from 0.636 m^3 to 0.642 m^3 , with an average of 0.640 m^3 , closely matching the actual volume. The sounding method measurements range from 0.540 m^3 to 0.609 m^3 , with an average of 0.573 m^3 , which is noticeably lower than the actual volume. This indicates that the 3D point cloud scanner system provides measurements that are much closer to the actual volume compared to

the traditional sounding method.

Table 4.8. Comparison of Volume Measurement Using the 3D Point Cloud Scanner System and Traditional Sounding Method for Different Surface Contours

Trials	Measured Volume (m^3)		Actual Volume (m^3)
	System	Sounding Method	
1	0.642	0.540	0.639
2	0.637	0.551	0.639
3	0.636	0.609	0.639
4	0.638	0.599	0.639
5	0.637	0.565	0.639
Average	0.640	0.573	

The comparison results demonstrate that the 3D Point Cloud Scanner System provides volume measurements that are consistent with those obtained using the traditional sounding method, regardless of the surface contour shape. The percentage differences between the two methods were minimal, indicating a high level of agreement.

The statistical analysis conducted for the comparison in table 4.8 is shown in appendix C, suggests since the p-value is less than 0.05, there is strong evidence to suggest that there is a significant difference between the sample mean of the sounding method data and the population mean of the system data. In other words, the sounding method measurements are significantly different from the system volume measurements.

4.3.3 System Evaluation

The system evaluation section provides a comprehensive assessment of the 3D Point Cloud Scanner System's performance based on the data obtained from various testing procedures.

4.3.3.1 LiDAR Calibration Evaluation

The evaluation of the LiDAR device and servo calibration revealed consistent performance across different ranges. The highest Mean Absolute Error (MAE) of 0.0351 meters was observed at a distance of 3 meters, while the lowest MAE of 0.01616 meters was recorded at 1.5 meters. Additionally, the average Standard Deviation of 0.0103 meters across the five different distances signifies consistent precision in measurements. These results demonstrate the accurate and precise performance of the LiDAR device in capturing range data across varying distances.

4.3.3.2 Servo Calibration Evaluation

The evaluation of the servo calibration revealed consistent performance across different angles. The highest Mean Absolute Error (MAE) was 0.6 degrees, while the lowest MAE was 0.2 degrees. These results indicate reliable performance in accurately positioning the servo motor, ensuring precise control over the scanning mechanism of the system.

4.3.3.3 Empty Storage Volume Measurement

The average measured volume across all trials was determined to be $1.00919\ m^3$, with an uncertainty of $\pm 0.0155\ m^3$. The gathered Mean Absolute Percentage Error (MAPE) was calculated to be $0.599377608\ %$, indicating the system's performance in accurately estimating the volume relative to the actual volume.

Additionally, the standard deviation of the measured volumes was determined to be $0.007835601\ m^3$, presenting consistency and precision of the system's volume measurements across multiple trials.

4.3.3.4 Different Volume Quantity Measurement

The system's performance achieved an average MAPE across the different volume quantity filled in the storage bin of $1.01308\ %$ and an average standard deviation $0.004691289\ m^3$, across the three conducted tests. This indicates that the system shows a consistent level of accuracy in measuring the volume of flour across different quantities. The average MAPE value of 1.01308% suggests a minor deviation from the actual volume, which is within an acceptable range for the intended application. Additionally, the average standard deviation of $0.004691289\ m^3$ reflects the precision and consistency of the system's volume measurements. Overall, these results demonstrate the system's capability to

accurately and reliably measure the volume of flour in varying storage capacities, providing valuable insights for its practical implementation and use.

4.3.3.5 Comparison Evaluation of the System and Sounding Method

These results validate the accuracy of the overall performance of the system and suggest that it is a reliable alternative to the traditional sounding method for measuring the volume of flour in storage bins. The system's ability to provide consistent and accurate measurements across different surface contours, combined with its automation for estimation of the volume, offers significant advantages over manual methods, particularly in terms of efficiency and reduction of human error.

CHAPTER V

CONCLUSION AND RECOMMENDATION

5.1 Conclusion

The study successfully designed and developed a web-based 3D point cloud scanner system capable of measuring the product volume inside a flour storage bin. The integration of the 3D point cloud scanner system and web application achieved the objectives. Promising results from testing the 3D Point Cloud Scanner System showed that it was capable of measuring the volume of flour materials in the storage bin with accuracy and the calibration result with statistical analysis emphasizing that the measured volume of the system has no significant difference between the known volume of the storage bin throughout the test. The system's accuracy and precision were further validated by comparing the volume measurements of the system to those of the traditional method, revealing a significant difference between the two methods. This suggests that the developed system is more accurate than the traditional method. Overall, the results demonstrate the system's potential for useful applications in monitoring storage capacity, as it can accurately estimate flour amounts under a variety of conditions.

5.2 Recommendations

In future studies, it may be consider using a LiDAR systems with multi-echo functionality. Such systems can effectively penetrate dust and other particles, allowing for continuous scanning even dust is present. Additionally, considering the computational limitations of the Raspberry Pi, researchers may opt for more powerful single-board computers to enhance processing speed and efficiency. By addressing these potential areas for improvement, future iterations of the system could offer enhanced performance and reliability in real-world applications.

BIBLIOGRAPHY

- Auat Cheein, F. A., Guivant, J., Sanz, R., Escolà, A., Yandún, F., Torres-Torriti, M., and Rosell-Polo, J. R. (2015). Real-time approaches for characterization of fully and partially scanned canopies in groves. *Computers and Electronics in Agriculture*, 118:361–371.
- Bewley, A., Shekhar, R., Leonard, S., Upcroft, B., and Lever, P. (2011). Real-time volume estimation of a dragline payload. In *2011 IEEE International Conference on Robotics and Automation*, pages 1571–1576.
- Bi, S., Yuan, C., Liu, C., Cheng, J., Wang, W., and Cai, Y. (2021). A survey of low-cost 3d laser scanning technology. *Applied Sciences*, 11(9).
- Bucklin, R., Thompson, S., Montross, M., and Abdel-Hadi, A. (2019). Chapter 9 - grain storage systems design. In Kutz, M., editor, *Handbook of Farm, Dairy and Food Machinery Engineering (Third Edition)*, pages 175–223. Academic Press, third edition edition.
- Bulut, S., Giese, T. G., Wende, M., and Anderl, R. (2020). The paperless factory: From document driven factories to model driven factories. In *2020 IEEE International Conference on Teaching, Assessment, and Learning for Engineering (TALE)*, pages 725–730.
- Chang, W.-C., Wu, C.-H., Tsai, Y.-H., and Chiu, W.-Y. (2017). Object volume

estimation based on 3d point cloud. In *2017 International Automatic Control Conference (CACS)*, pages 1–5.

Chua, C. K., Wong, C. H., and Yeong, W. Y. (2017). Chapter four - software and data format. In Chua, C. K., Wong, C. H., and Yeong, W. Y., editors, *Standards, Quality Control, and Measurement Sciences in 3D Printing and Additive Manufacturing*, pages 75–94. Academic Press.

Clar, S. E. and Salaan, C. J. O. (2022). Volume estimation using convex hull method for point cloud-based materials inside a silo.

Duff, E. (2000). Automated volume estimation of haul-truck loads.

Duysak, H. and Yigit, E. (2020). Machine learning based quantity measurement method for grain silos. *Measurement*, 152:107279.

Graham, R. L. and Frances Yao, F. (1983). Finding the convex hull of a simple polygon. *Journal of Algorithms*, 4(4):324–331.

Guevara, J., Arevalo-Ramirez, T., Yandun, F., Torres-Torriti, M., and Cheein, F. A. (2020). Point cloud-based estimation of effective payload volume for earthmoving loaders. *Automation in Construction*, 117:103207.

Jaboyedoff, M., Oppikofer, T., Abellán, A., Derron, M.-H., Loyer, A., Metzger, R., and Pedrazzini, A. (2012). Use of lidar in landslide investigations: a review. *Natural Hazards*, 61(1):5–28.

- Jeong, D., Li, Y., Lee, H. J., Lee, S. M., Yang, J., Park, S., Kim, H., Choi, Y., and Kim, J. (2018). Efficient 3d volume reconstruction from a point cloud using a phase-field method. *Mathematical Problems in Engineering*, 2018:7090186.
- Kang, X., Yin, S., and Fen, Y. (2018). 3d reconstruction & assessment framework based on affordable 2d lidar. In *2018 IEEE/ASME International Conference on Advanced Intelligent Mechatronics AIM*, pages 292–297.
- Kim, Y. (2002). Convex hull ensemble machine. In *2002 IEEE International Conference on Data Mining, 2002. Proceedings.*, pages 243–249.
- Kumar, D. and Kalita, P. (2017). Reducing postharvest losses during storage of grain crops to strengthen food security in developing countries. *Foods*, 6(1).
- Lim, J. Z. (2019). *Cloud Based Ros Implementation for Indoor Robot*. PhD thesis, UTAR.
- Liu, Y. and Zheng, Y. (2021). Accurate volume calculation driven by delaunay triangulation for coal measurement. *Scientific Programming*, 2021:6613264.
- Maus, A. (1984). Delaunay triangulation and the convex hull ofn points in expected linear time. *BIT Numerical Mathematics*, 24(2):151–163.
- Meng, X., Wang, T., Cheng, D., Su, W., Yao, P., Ma, X., and He, M. (2023).

- Enhanced point cloud slicing method for volume calculation of large irregular bodies: Validation in open-pit mining. *Remote Sensing*, 15(20).
- Munarso, S. J., Widayanti, S. M., and Qanytah (2022). Advances in postharvest technology and its implementation. *IOP Conference Series: Earth and Environmental Science*, 1024(1):012001.
- Ocando, M. G., Certad, N., Alvarado, S., and Terrones, Á. (2017). Autonomous 2d slam and 3d mapping of an environment using a single 2d lidar and ros. In *2017 Latin American Robotics Symposium (LARS) and 2017 Brazilian Symposium on Robotics (SBR)*, pages 1–6.
- Putman, E. B. and Popescu, S. C. (2018). Automated estimation of standing dead tree volume using voxelized terrestrial lidar data. *IEEE Transactions on Geoscience and Remote Sensing*, 56(11):6484–6503.
- Qureshi, B., Koubaa, A., Sriti, M.-F., Javed, Y., and Alajlan, M. (2016). Poster: Dronemap-a cloud-based architecture for the internet-of-drones. In *EWSN*, pages 255–256.
- Raba, D., Gurt, S., Vila Clarà, O., and Farrés, E. (2020). An internet of things (iot) solution to optimise the livestock feed supply chain. pages 103–118.
- Raj, T., Hashim, F., Huddin, A., Ibrahim, M. F., and Hussain, A. (2020). A survey on lidar scanning mechanisms. *Electronics*, 9:741.

- Rhee, J. H., Kim, S. I., Lee, K. M., Kim, M. K., and Lim, Y. M. (2021). Optimization of position and number of hotspot detectors using artificial neural network and genetic algorithm to estimate material levels inside a silo. *Sensors*, 21(13).
- Rusu, R. B. and Cousins, S. (2011). 3d is here: Point cloud library (pcl). In *2011 IEEE International Conference on Robotics and Automation*, pages 1–4.
- Sarker, V. K., Qingqing, L., and Westerlund, T. (2020). 3d perception with low-cost 2d lidar and edge computing for enhanced obstacle detection. In *2020 IEEE Conference on Industrial Cyberphysical Systems (ICPS)*, volume 1, pages 49–54.
- St-Onge, D. and Herath, D. (2022). *The Robot Operating System (ROS1 &2): Programming Paradigms and Deployment*, pages 105–126. Springer Nature Singapore, Singapore.
- Stojanovic, V. (2023). Point cloud analytics: Proposed future work. *Proceedings of the HPI Research School on Service-oriented Systems Engineering 2020 Fall Retreat*, page 137.
- Turner, A., Jackson, J., Koeninger, N., Mcneill, S., Montross, M., Casada, J., Boac, R., Bhadra, R., Maghirang, S., and Thompson (2017). Stored grain volume measurement using a low density point cloud. *Applied Engineering in Agriculture*, 33:105–112.

- Turner, A., Jackson, J., Koeninger, N., Mcneill, S., Montross, M., Casada, M., Boac, J., Bhadra, R., Maghirang, R., and Thompson, S. (2016). Error analysis of stored grain inventory determination. *Transactions of the ASABE (American Society of Agricultural and Biological Engineers)*, 59:1061–1072.
- Vogt, M. and Gerding, M. (2017). Silo and tank vision: Applicaltions, challenges, and technical solutions for radar measurement of liquids and bulk solids in tanks and silos. *IEEE Microwave Magazine*, 18(6):38–51.
- Wang, Q. and Kim, M.-K. (2019). Applications of 3d point cloud data in the construction industry: A fifteen-year review from 2004 to 2018. *Advanced Engineering Informatics*, 39:306–319.
- Yegorova, S. V., Slavyanskiy, A. A., Postnikova, T. A., Pereboev, A. V., Mazanova, G. V., and Murzakov, M. G. (2021). Improving the technology of post-harvest processing and storage of grain raw materials at the enterprises of the grain processing industry. *IOP Conference Series: Earth and Environmental Science*, 640(2):022040.
- Yigit, E., İsiker, H., Toktas, A., and Tjuatja, S. (2015). Cs-based radar measurement of silos level. In *2015 IEEE International Geoscience and Remote Sensing Symposium (IGARSS)*, pages 3746–3749.
- Yuan, C., Bi, S., Cheng, J., Yang, D., and Wang, W. (2021). Low-cost cali-

bration of matching error between lidar and motor for a rotating 2d lidar.

Applied Sciences, 11(3).

Zhi, Y., Zhang, Y., Chen, H., Yang, K., and Xia, H. (2016). A method of 3d point cloud volume calculation based on slice method. In *Proceedings of the 2016 International Conference on Intelligent Control and Computer Application*, pages 155–158. Atlantis Press.

APPENDIX A

COMPONENTS SPECIFICATION

YDLiDAR Model X4

1 PRODUCT OVERVIEW

YDLIDAR X4 is a 360 degrees 2D LiDAR (hereinafter referred to as X4) developed by EAI team. Based on the principle of triangulation, it is equipped with related optics, electricity, and algorithm design to achieve high-frequency and high-precision distance measurement. The mechanical structure rotates 360 degrees to continuously output the angle information as well as the point cloud data of the scanning environment while ranging.

1.1 Product Features

- 360 degrees scan ranging
- High accuracy, stable performance
- Wide measuring range
- Strong resistance to ambient light interference
- Low power consumption, small size, stable performance and long service life
- Class I eye safety
- Motor speed is adjustable, the proposed speed is 6~12Hz
- High-speed ranging, ranging frequency up to 5kHz

1.2 Applications

- Robot navigation and obstacle avoidance
- Robot ROS teaching and research
- Regional security
- Environmental scanning and 3D reconstruction
- Navigation and obstacle avoidance of home robots/ robot vacuum cleaners

1.3 Installation and Dimensions

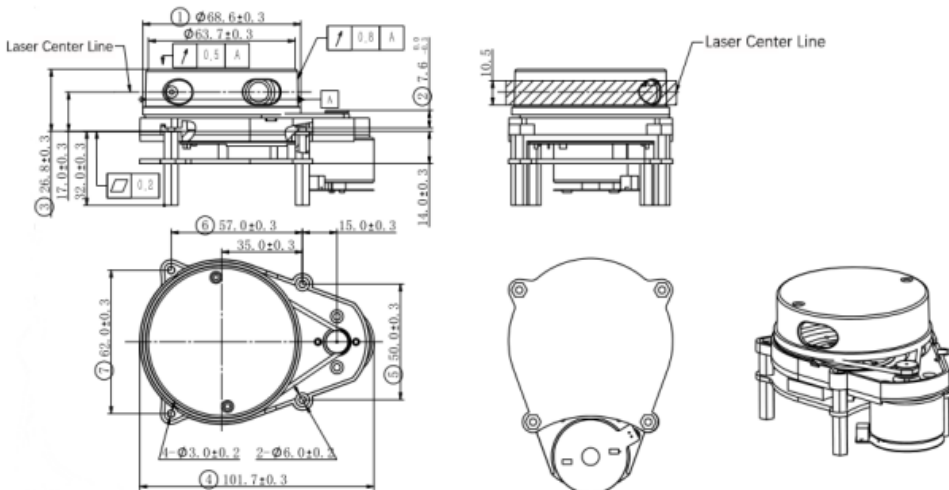


FIG 1 YDLIDAR X4 INSTALLATION AND MECHANICAL DIMENSIONS (UNIT:MM)

2 SPECIFICATIONS

2.1 Performance Parameter

CHART 1 YDLIDAR X4 PRODUCT PARAMETER

Item	Min	Typical	Max	Unit	Remarks
Ranging frequency	/	5000	/	Hz	Ranging 5000 times per second
Motor frequency	6	/	12	Hz	PWM or voltage speed regulation
Ranging distance	0.12	/	10	m	Indoor environment with 80% Reflectivity
Field of view	/	0-360	/	Deg	/
Systematic error	/	2	/	cm	Range ≤ 1m
Relative error	/	3.5%	/	/	1m < Range ≤ 6m
Tilt angle	0.25	1	1.75	Deg	/
Angle resolution	0.43 (frequency@ 6Hz)	0.50 (frequency@ 7Hz)	0.86 (frequency@ 12Hz)	Deg	Different motor frequency

Note 1: The measurement range and relative accuracy above are the factory FQC standard value based on 80% reflectivity object.

Note 2: The relative error value indicates the accuracy of the Lidar measurement. Relative error (mean value) = (average measured distance-actual distance)/actual distance *100%, sample size: 100pcs.

Note 3: Lidar is a precision device. Please avoid using Lidar under high or low temperature or strong vibration situation, which might cause an exceeded relative error.

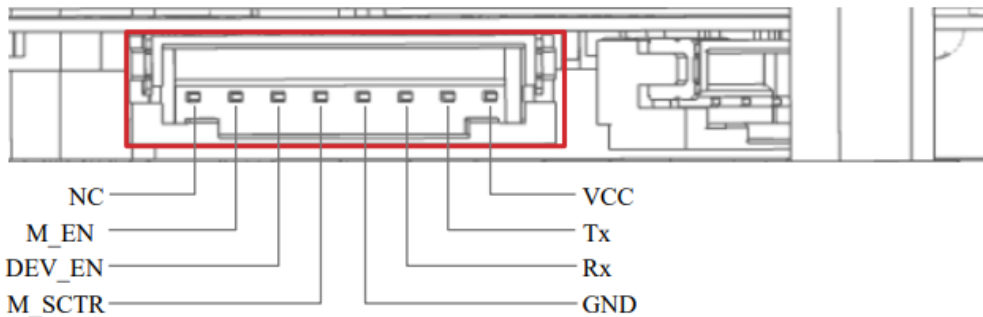


FIG 2 YDLIDAR X4 INTERFACES

CHART 3 YDLIDAR X4 INTERFACE DEFINITION

Pin	Type	Description	Defaults	Range	Remarks
VCC	Power supply	Positive	5V	4.8V-5.2V	/
Tx	Output	System serial port output	/	/	Data stream: LiDAR→Peripherals
Rx	Input	System serial port input	/	/	Data stream: Peripherals→LiDAR
GND	Power supply	Negative	0V	0V	/
M_EN	Input	Motor enables control terminal	3.3V	0V-3.3V	High level enables
DEV_EN	Input	Ranging enable control terminal	3.3V	0V-3.3V	High level enables
M_SCTR	Input	Motor speed control terminal	1.8V	0V-3.3V	Voltage speed regulation or PWM speed regulation
NC	/	Reserve pin	/	/	/

2.4 Data Communication

With a 3.3V level serial port (UART), users can connect the external system and the product through the physical interface. After that, users can obtain the real-time scanned point cloud data, device information as well as device status. The communication protocol of parameters are as follows:

AX-12A Servo Motor



| AX-12+, AX-12A

1. Specifications

Item	Specifications
Baud Rate	7,843 [bps] ~ 1 [Mbps]
Weight	AX-12 (53.5 [g]), AX-12+ (53.5 [g]), AX-12A (54.6 [g])
Dimensions (W x H x D)	32 X 50 X 40 [mm] 1.26 X 1.97 X 1.57 [inch]
Resolution	0.29 [°]
Running Degree	0 ~ 300 [°] Endless Turn
Motor	Cored
Gear Ratio	254 : 1
Stall Torque	1.5 [N.m] (at 12 [V], 1.5 [A])
No Load Speed	59 [rev/min] (at 12V)
Operating Temperature	-5 ~ +70 [°C]
Input Voltage	9.0 ~ 12.0 [V] (Recommended : 11.1V)
Command Signal	Digital Packet
Physical Connection	TTL Level Multi Drop Bus Half Duplex Asynchronous Serial Communication (8bit, 1stop, No Parity)
ID	254 ID (0~253)
Feedback	Position, Temperature, Load, Input Voltage, etc
Gear Material	Engineering Plastic(Full)
Case Material	Engineering Plastic(Front, Middle, Back)

NOTE : Stall torque is the maximum instantaneous and static torque. Stable motions are possible with robots designed for loads with 1/5 or less of the stall torque.

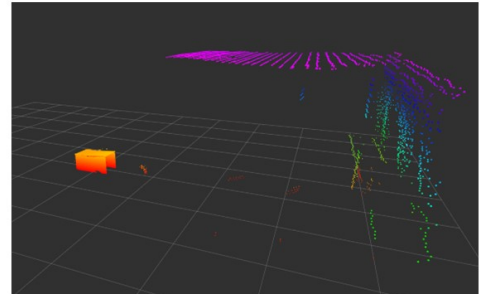
Specifications

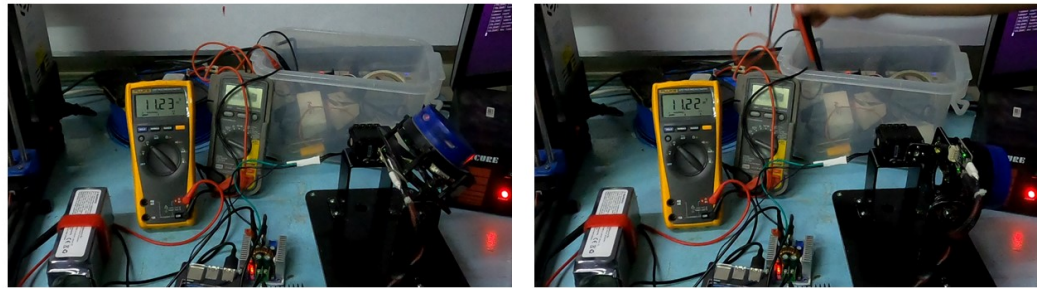
Broadcom BCM2711, Quad core Cortex-A72 (ARM v8) 64-bit SoC @ 1.8GHz
1GB, 2GB, 4GB or 8GB LPDDR4-3200 SDRAM (depending on model)
2.4 GHz and 5.0 GHz IEEE 802.11ac wireless, Bluetooth 5.0, BLE
Gigabit Ethernet
2 USB 3.0 ports; 2 USB 2.0 ports.
Raspberry Pi standard 40 pin GPIO header (fully backwards compatible with previous boards)
2 x micro-HDMI® ports (up to 4kp60 supported)
2-lane MIPI DSI display port
2-lane MIPI CSI camera port
4-pole stereo audio and composite video port
H.265 (4kp60 decode), H264 (1080p60 decode, 1080p30 encode)
OpenGL ES 3.1, Vulkan 1.0
Micro-SD card slot for loading operating system and data storage
5V DC via USB-C connector (minimum 3A*)
5V DC via GPIO header (minimum 3A*)
Power over Ethernet (PoE) enabled (requires separate PoE HAT)
Operating temperature: 0 – 50 degrees C ambient

APPENDIX B

TESTING DOCUMENTATION

COMPONENT TESTING AND CALIBRATION

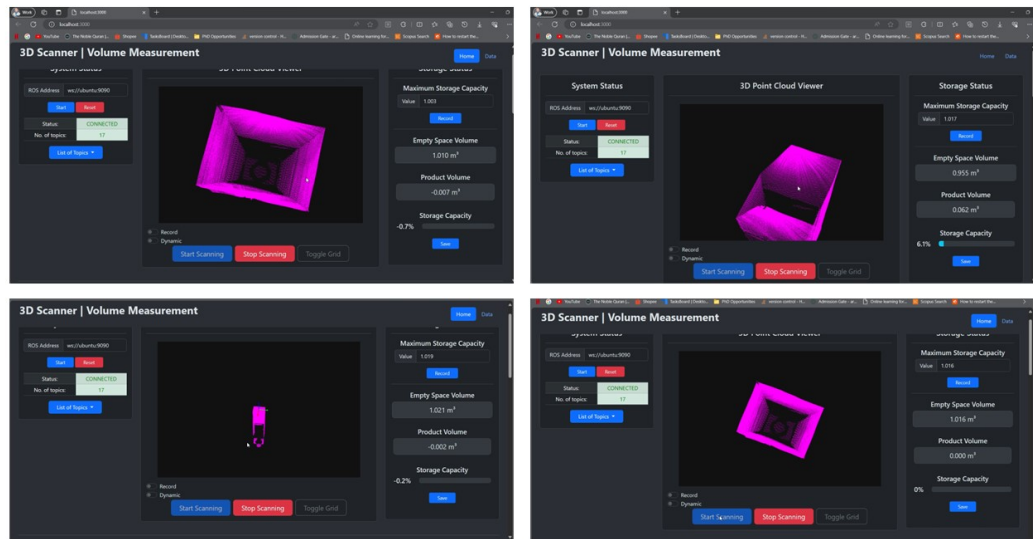
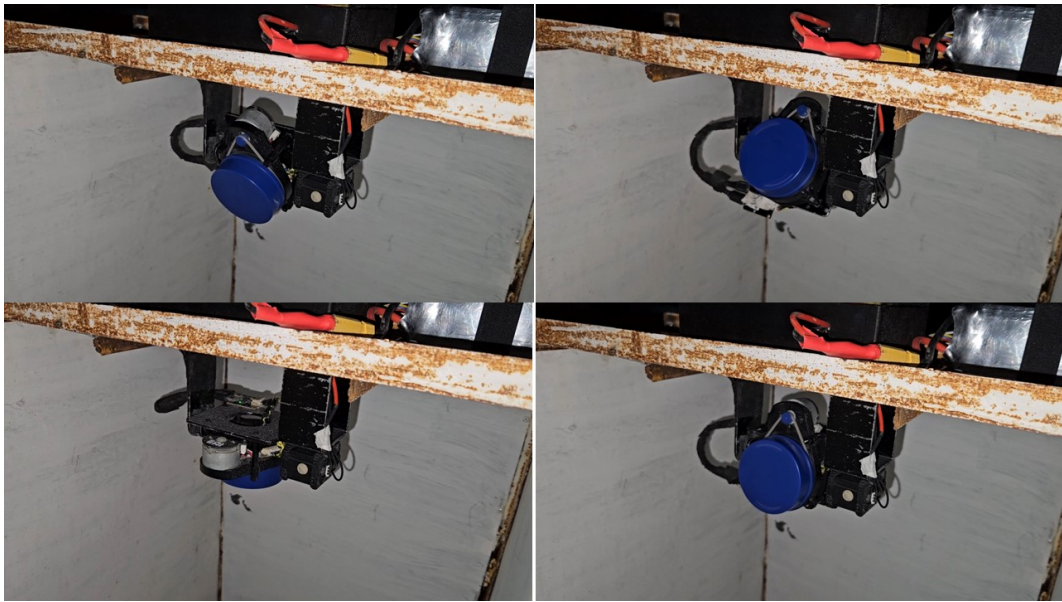


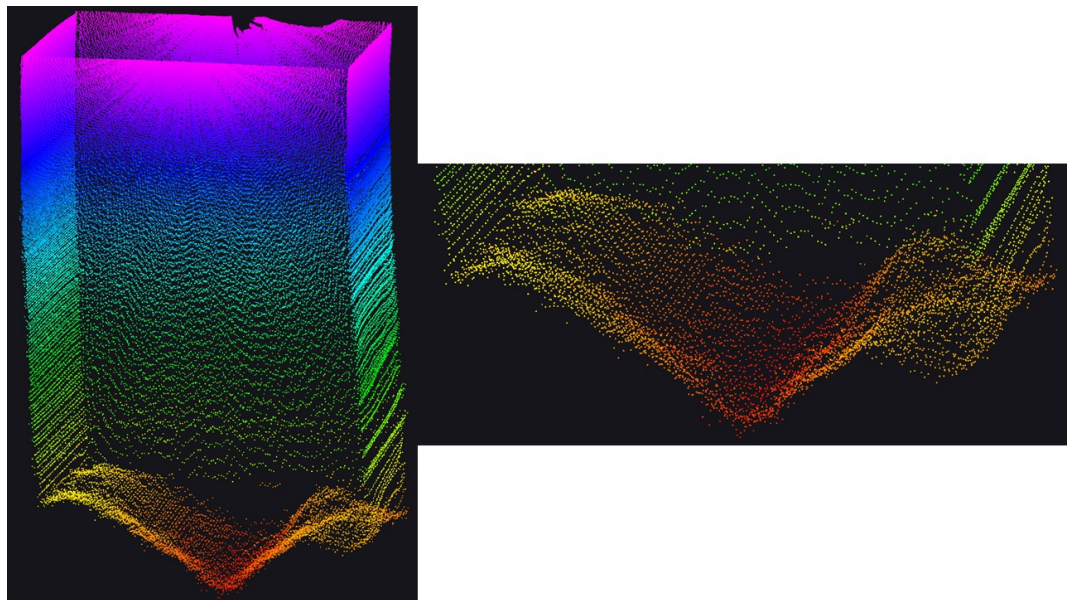


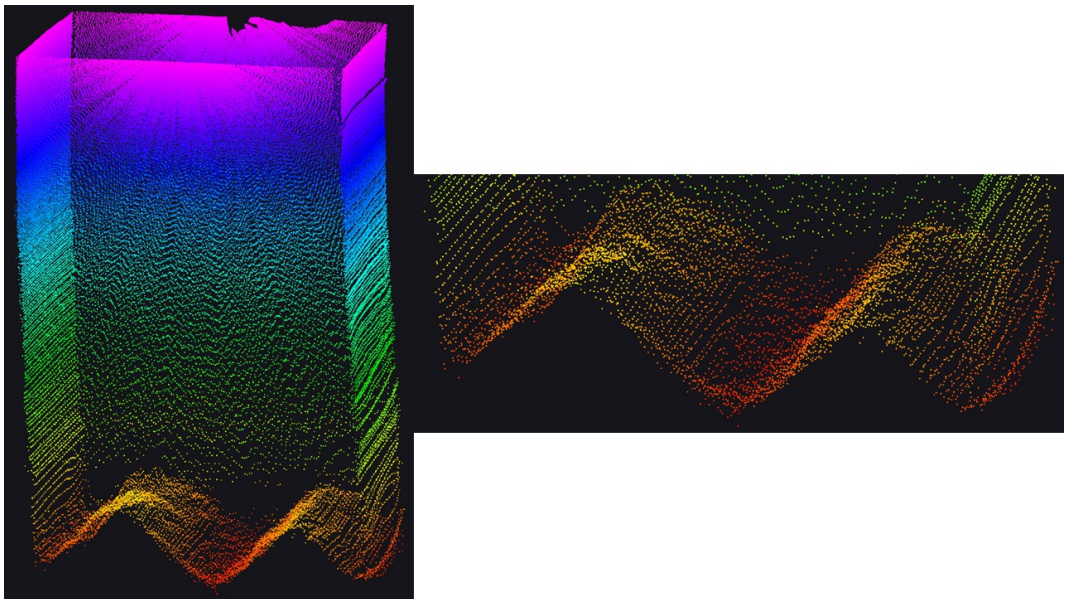
ACTUAL TESTING

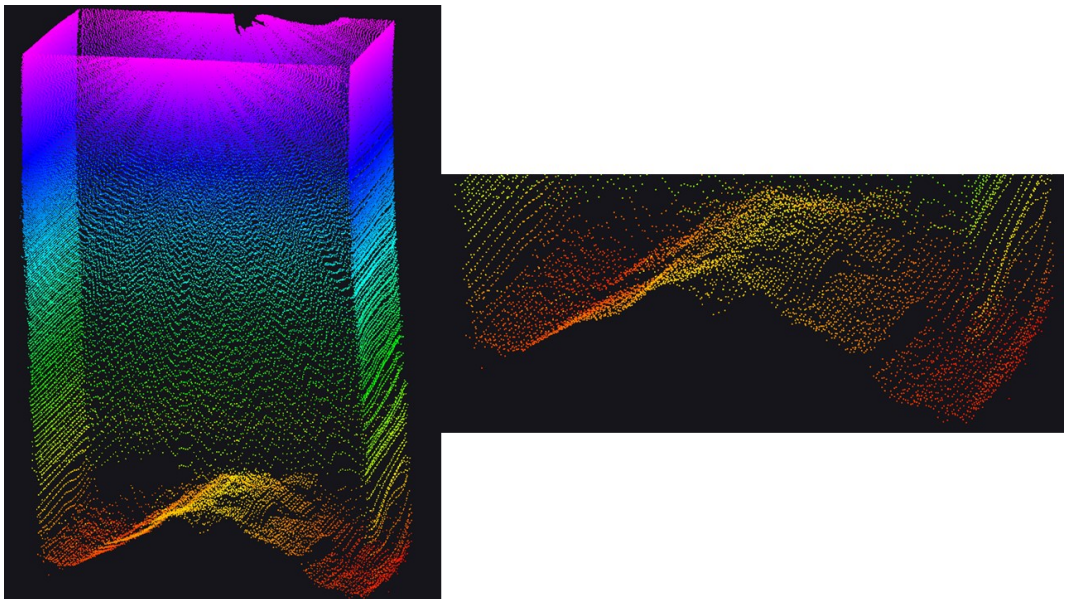


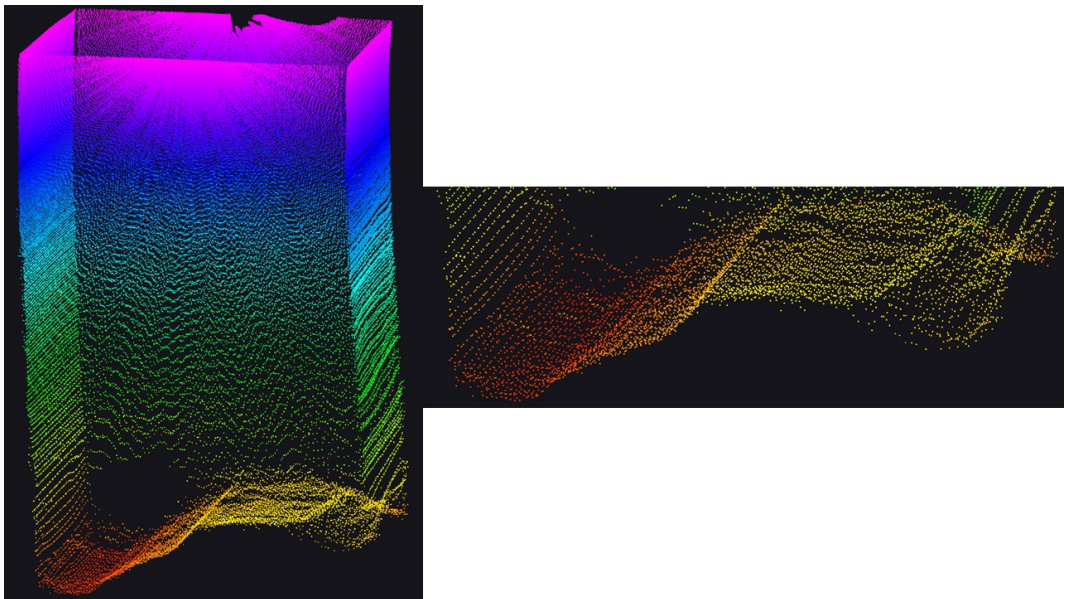


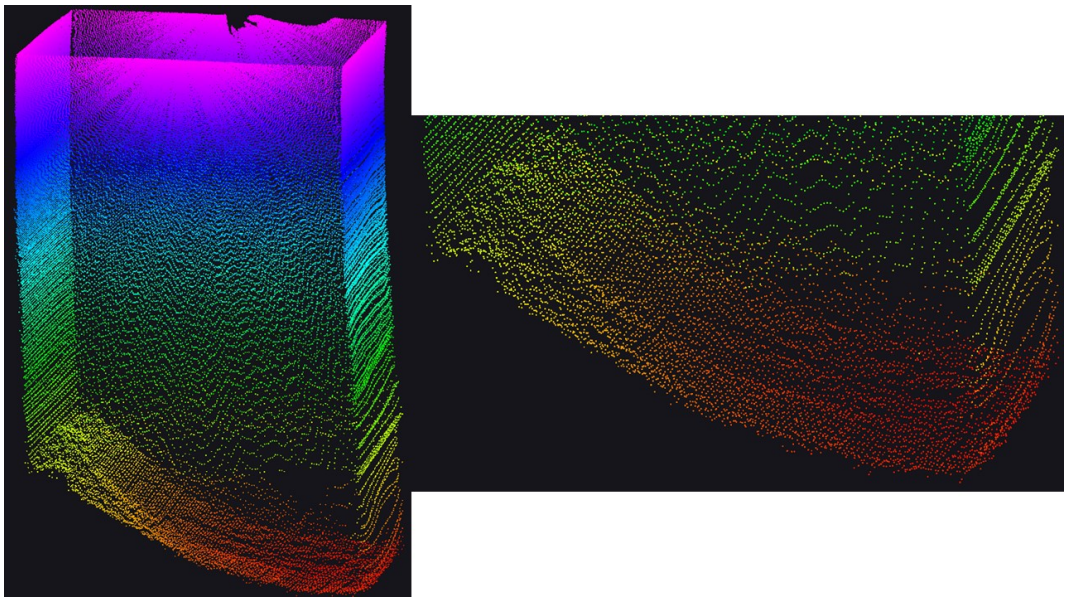


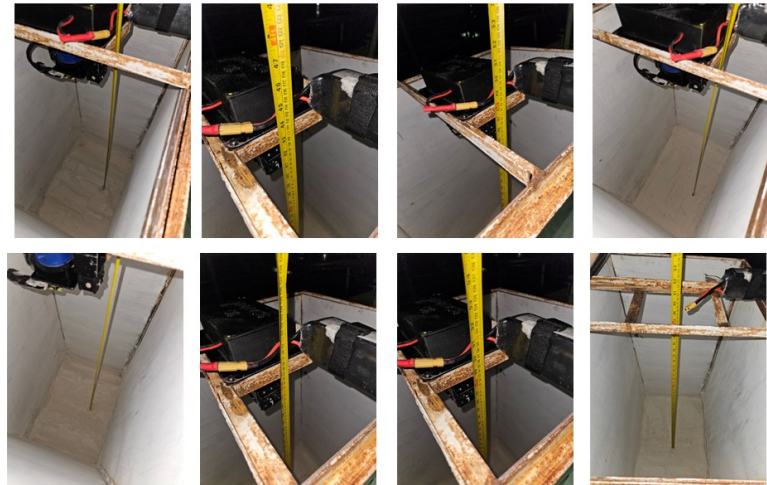
System and Sounding Method Actual Testing**CONTOUR 1**

CONTOUR 2

CONTOUR 3

CONTOUR 4

CONTOUR 5

SOUNDING METHOD

APPENDIX C

STATISTICAL DATA

Table C.1. One Sample-test for Actual and Measured Volume of Empty Storage Bin Volume Measurement Result

Estimate	Statistic	P Value	Parameter	Conf. Low	Conf. High	Method	Alternative
1.013	-0.390	0.699	36.000	1.012	1.013	One Sample-test	Two Sided

Table C.2. ANOVA Results of Volume Measurements Calibration Result of the System Across Two Contours with A Known Volume of $0.0594\ m^3$

	Df	Sum Sq	Mean Sq	F value	Pr(F)
Variable	2.0000	0.0000	0.0000	3.1089	0.0817
Residuals	12.0000	0.0000	0.0000		

Table C.3. ANOVA Results of Volume Measurements Calibration Result of the System Across Two Contours with A Known Volume of $0.4752\ m^3$

	df	sumsq	meansq	statistic	p.value
Variable	2.0000	0.0000	0.0000	1.2042	0.3337
Residuals	12.0000	0.0000	0.0000		

Table C.4. ANOVA Results of Volume Measurements Calibration Result of the System Across Two Contours with A Known Volume of $0.7128\ m^3$

	df	sumsq	meansq	statistic	p.value
Variable	2.0000	0.0001	0.0000	4.0233	0.07323
Residuals	12.0000	0.0000	0.0000		

Table C.5. One Sample-test for Comparison of Volume Measurement of the System VS. Sounding Method

Estimate	Statistic	P Value	Parameter	Conf. Low	Conf. High	Method	Alternative
0.573	-5.003	0.007	5	0.536	0.610	One Sample-test	Two Sided

CERTIFICATE OF AUTHENTIC AUTHORSHIP

I hereby declare that this submission is my own work and, to the best of my knowledge, it contains no materials previously published nor written by another person. This work does not also contain material which, to a substantial extent, has been accepted for an award of any other degree or diploma, except where due acknowledgement is made in the manuscript. Any contribution made to the research by others, with whom I have worked at MSU-IIT or elsewhere, is explicitly acknowledged in the manuscript.

I also declare that the intellectual content of this manuscript is the product of my own work, except the assistance I received in the project's design, conception and style, presentation and linguistic expression which I also acknowledge.

JAAFAR J. OMAR
Author